Visible-light-driven organic transformations on semiconductors

Guanqun Han, Yujie Sun[*]

Department of Chemistry, University of Cincinnati, Cincinnati, OH 45221, USA

ARTICLE INFO

ABSTRACT

Along with the increasing interest in exploring green and sustainable approaches in organic synthesis, photon, the cleanest energy form, has been widely utilized in driving various organic transformations. In contrast to well-established organic photocatalysis utilizing homogeneous photosensitizers and photo-catalysts, solid-state semiconductors have received less but rapidly growing interest in this field. Herein, we summarize recent development in organic photocatalysis utilizing semiconductor-based photo-catalysts, including metal oxides, metal chalcogenides, and metal-free carbon nitrides. For each category of semiconductors, both oxidation and reduction organic reactions are introduced first, followed by redox coupled reactions utilizing both excited electrons and holes. At the end, the remaining challenges and future opportunities of this field are discussed.

1. Introduction

Rapid growth of energy demands and the detrimental impact of fossil fuel utilization on environment have triggered intense research efforts in the exploration of clean and renewable energy [1]. Sunlight, as one of the greenest and most abundant energy sources, possesses great potential. Since the discovery of photo-electrochemical water splitting on a TiO$_2$ semiconductor electrode by Fujishima and Honda in 1972 [2], photocatalysis has gained significant advancement and emerged as a promising approach for the generation of chemical fuels (*e.g.*, H$_2$ from water splitting and CH$_4$ from CO$_2$ reduction) utilizing photons as the sole energy input. In addition to fuel production, photocatalysis is also a powerful tool in driving chemical synthesis in an environmentally benign manner.

Since the pioneering work of the MacMillan group, photo-catalysis emerged as a popular approach in organic synthesis. A lot of elegant work have been developed utilizing homogeneous photocatalysts, such as ruthenium- and iridium-based metal complexes and metal-free organic dyes [3]. Compared to these homogeneous counterparts, semiconductor-based photocatalysts have several advantages, including tunable band gap, easy sepa-ration from the reaction mixture (phase separation), and possible recyclability. However, semiconductor-based photocatalysis has

been considered as an unselective process for a long time, espe-cially in H$_2$O, due to the generation of free radical intermediates ($\cdot$OH, O$_2^{\cdot-}$, and HO$_2\cdot$). Therefore, a lot of efforts have been devoted to developing selective organic transformations on semiconductors.

Generally, three steps are involved in semiconductor-based photocatalysis: (i) light absorption and the generation of excited electron (e$^-$) $-$ hole (h$^+$) pairs in which electrons in the valence band will migrate to the conduction band, (ii) separation and migration of the above generated e$^-$-h$^+$ pairs, and (iii) utilization of the excited species including reduction reactions driven by excited electrons and oxidation reactions by remaining holes.

To guarantee the success of organic transformations, several criteria should be met: (i) the photon energy of the incident light should be larger than the band-gap energy of the semiconductor, (ii) the band maximum positions need to cover the potential gap between two desired half reactions, (iii) the lifetime of the excited species should be on the same time-scale with redox reactions, (iv) the semiconductor needs to provide sufficient active surface sites for organic reactions to take place, and (v) the semiconductor should be stable for practical application. The most commonly used TiO$_2$ is a promising semiconductor for organic transformations, especially for oxidation reactions due to its wide band gap (3.2 eV) and high valence band position. However, exactly because of its wide band gap, TiO$_2$ can only absorb ultraviolet (UV) light irradia-tion. In order to encompass the major component of solar irradia-tion, it is highly desirable to develop visible-light-absorbing semiconductors in that visible light accounts for 43% of the

* Corresponding author.
E-mail address: yujie.sun@uc.edu (Y. Sun).

incoming solar spectrum. Recent years have witnessed the rapid development of the selective formation of value-added organic molecules through oxidation, reduction, or redox coupled reactions via semiconductor-based photocatalysts under visible light irradiation [4]. This minireview aims to present the achievement of photocatalytic organic reactions on visible light-responsive semiconductors in the last decade and provides our personal perspective at the end, in the hope of generating increasing interest in this fruitful field.

2. Photocatalytic reactions of organic compounds on metal oxide semiconductors

Semiconductors have long been recognized as promising photocatalysts for a variety of reactions. Among many semiconductor candidates, TiO_2 is likely the most investigated for organic transformations. However, due to its wide band gap (~3.2 eV), TiO_2 is only able to absorb ultraviolet light ($\lambda_{abs} < 385$ nm), largely limiting its application scope. In order to extend its absorption spectrum towards the visible light region, two promising strategies have been frequently adopted: (i) decoration of visible-light-absorbing dyes and (ii) introduction of metal or non-metal co-catalysts. Since most photocatalytic organic reactions can be categorized as either oxidative or reductive transformations, hereby we will first introduce visible-light-driven organic oxidation reactions on TiO_2-based photocatalysts followed by reduction reactions. In the end, several redox-coupled reactions on metal oxide utilizing both excited electrons and holes are summarized.

2.1. Organic oxidative transformations via metal oxide-based photocatalysts

The decoration of visible light responsive organic dyes has been considered as a promising method to enhance the visible light absorption of metal oxides. Alizarin red S (ARS, Fig. 1a) is an organic dye and the pinnacle of visible light absorption of ARS adsorbed on TiO_2 (ARS-TiO_2) is around 500 nm. Through the binding between the catechol groups of ARS and the surface hydroxy groups of TiO_2, such prepared ARS-TiO_2 was reported to accomplish the aerobic oxidation of organic sulfides to sulfoxides (Fig. 1b) [5]. In this work, a redox mediator TEMPO was also found to play an important role, not only stabilizing the anchored dye but also facilitating the overall photocatalytic activity. Such a photocatalytic system consisting of ARS-TiO_2, TEMPO, and O_2 was able to drive the desirable oxidation for a wide scope of substrates. The reaction mechanism was also proposed and outlined in Fig. 1c. The decoration of ARS on TiO_2 enables visible light absorption ($\lambda_{abs} > 450$ nm) and the light-excited ARS* transfers electrons to the conduction band of TiO_2 while itself forms ARS$^{+\cdot}$. Subsequently, the excited electrons in the TiO_2 conduction band reduce O_2 to $O_2^{-\cdot}$ while ARS$^{+\cdot}$ oxidizes TEMPO to TEMPO$^+$, both of which synergistically react with organic sulfides to yield sulfoxide.

Besides sulfide oxidation, ARS-TiO_2 is also able to drive the oxidation of many other substrates, such as amines and alcohols [6]. For example, Lang et al. applied the ARS-TiO_2 system for the selective oxidation of benzyl alcohol to benzaldehyde [7]. Unlike the above sulfide oxidation, in which TEMPO played a central role for the high selectivity, no redox mediator was required to achieve the excellent selectivity for alcohol oxidation. Other organic dyes like eosin Y, thionine, and flavin (Fig. 2a) were also evaluated. Except thionine, all the other candidates were proved to be competent dyes on TiO_2 for the selective oxidation of benzyl alcohol to benzaldehyde with a selectivity up to 98% under green LED irradiation (Fig. 2b). Among these four dyes, ARS was demonstrated to exhibit the best performance.

In addition to the oxidation of sulfides and alcohols, aerobic photocyanation of tertiary amines was also reported on dye-sensitized TiO_2 [8]. The desirable products are the corresponding
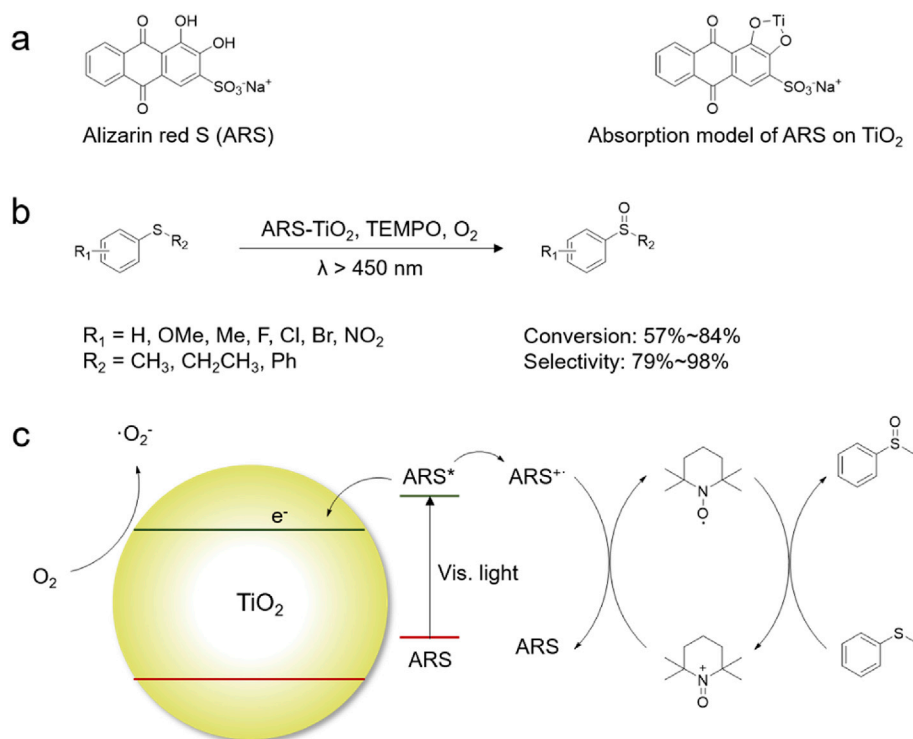

Fig. 1. (a) Molecular structure of organic dye ARS and a possible absorption model of ARS-TiO_2. (b) Reaction pathway from organic sulfides to sulfoxides. (c) Proposed reaction scheme of aerobic oxidation of thioanisole catalyzed by ARS-TiO_2 with TEMPO as a redox mediator.
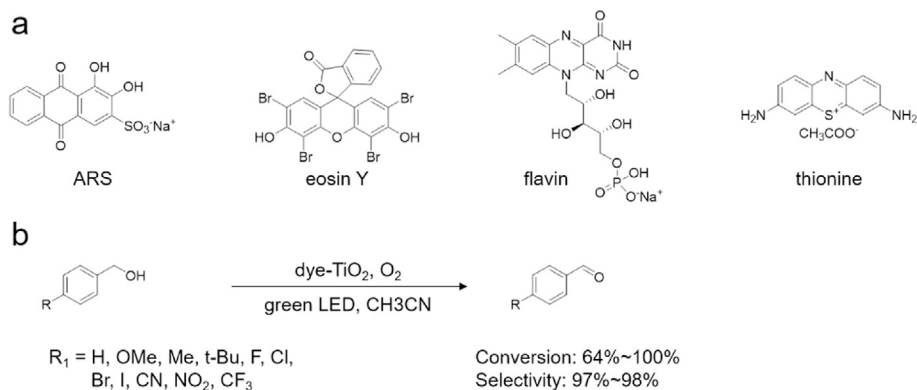
Fig. 2. (a) Molecular structures of four representative organic dyes. (b) Reaction pathway of the photocatalytic oxidation of benzyl alcohol to benzaldehyde.
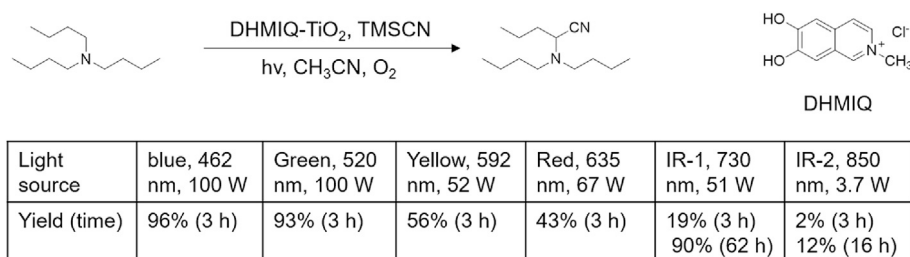

Light source	blue, 462 nm, 100 W	Green, 520 nm, 100 W	Yellow, 592 nm, 52 W	Red, 635 nm, 67 W	IR-1, 730 nm, 51 W	IR-2, 850 nm, 3.7 W
Yield (time)	96% (3 h)	93% (3 h)	56% (3 h)	43% (3 h)	19% (3 h) 90% (62 h)	2% (3 h) 12% (16 h)

Fig. 3. Reaction pathway of the photocatalytic oxidative cyanation of tributylamine on DHMIQ-TiO$_2$. The included table presents the product yields obtained under different conditions.

α-aminonitriles, which are useful intermediates for the synthesis of nitrogen-containing bioactive compounds. The utilized organic dye was 6,7-dihydroxy-2-methylisoquinolinium (DHMIQ) which contained a redox-active catechol group for anchoring on the surface of TiO$_2$. The addition of DHMIQ significantly enhanced its absorption in the visible light region and even near the near-IR range, consequently resulting in much improved reaction efficiency (Fig. 3). Other dye-sensitized TiO$_2$ systems, such as eosin Y-TiO$_2$ [9] and Ru(II)-erythrosine B/TiO$_2$ [10], were also developed to drive the photocatalytic oxidation of benzyl ethers to benzoates (Scheme 1) and C–H olefination of arene carboxylic acids (Scheme 2), respectively. Since ZnO has a similar band gap as that of TiO$_2$, dye sensitized-ZnO has also been investigated for visible-light-driven organic transformations, such as alcohol oxidation (Scheme 3)

[11]. It was found that under the same condition dye sensitized-ZnO exhibited better activity for the aldehyde formation relative to the TiO$_2$ system, which was rationalized by the strong back electron transfer in the TiO$_2$/ARS system.

Another effective strategy in enhancing the visible light absorption of metal oxides is metal or nonmetal decoration. Au, Ag, and Cu are considered as effective metal dopants as their absorption spectra are within the visible light region, which arise from the surface plasmon resonance effect-a resonant oscillation of electrons coupled with photons [12]. A large group of metal oxides have been investigated as substrates to host plasmonic dopants, including TiO$_2$, CeO$_2$, ZrO$_2$, Al$_2$O$_3$, SiO$_2$, etc, among which TiO$_2$ is the most popular choice. For instance, a mixture of anatase/rutile TiO$_2$ (Degussa, P25) was utilized to support Au nanoparticles Au$_2$(DP$_{673}$)
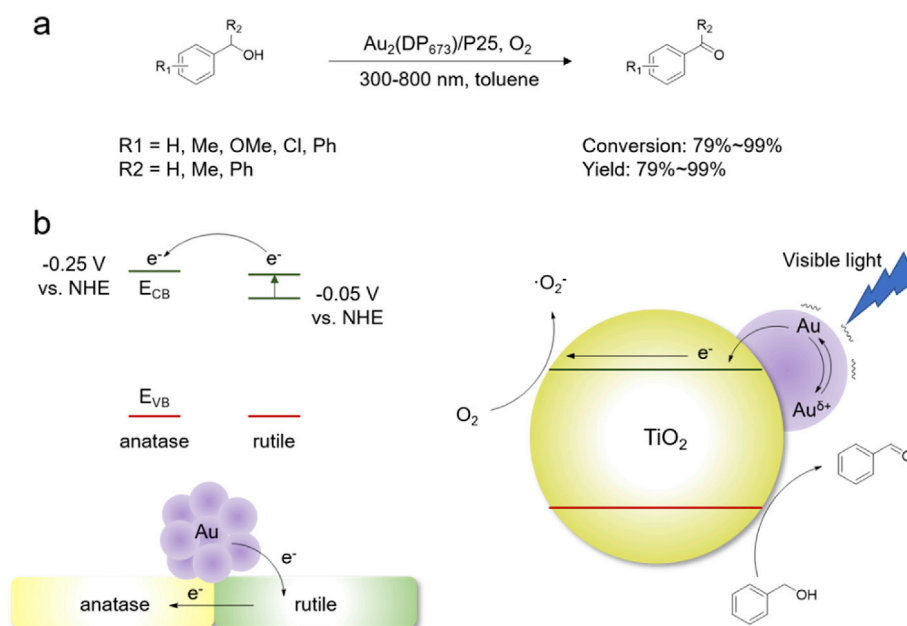

Yield: 65%~91%

Scheme 1.

Yield: 36%~84%
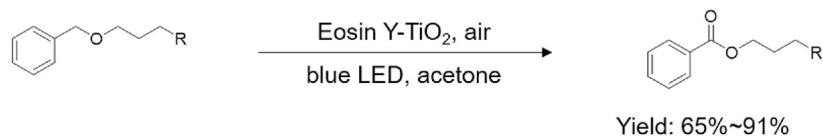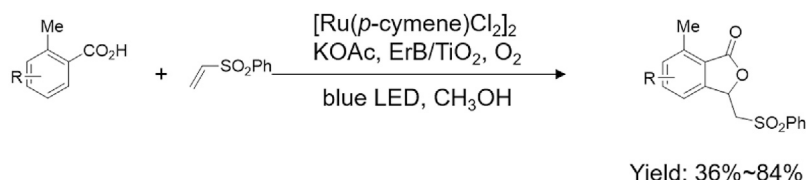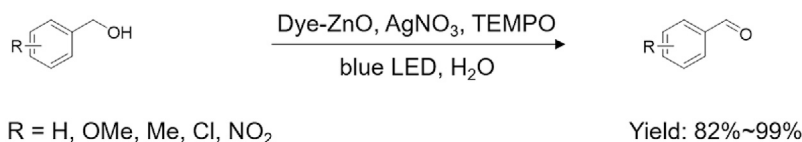
Scheme 2.

Scheme 3.

Fig. 4. (a) Reaction pathway and (b) proposed mechanism of aromatic alcohol oxidation on the Au$_2$(DP$_{673}$)/P25 photocatalyst.
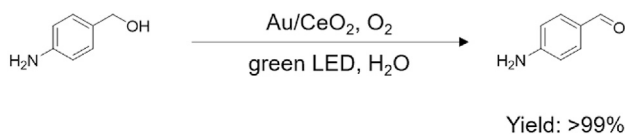
and the resulting Au$_2$(DP$_{673}$)/P25 photocatalyst could drive the aerobic oxidation of alcohols to the corresponding carbonyls with high yields (79%–99%) under solar irradiation (Fig. 4a) [13]. It has been demonstrated that those small Au nanoparticles (<5 nm) located at the interface between anatase and rutile acted as the active sites. Upon solar irradiation, excited electrons transferred from the activated Au nanoparticles to rutile and accumulated in its conduction band, which would shift the valence band of rutile to a more negative position and result in further electron transfer to anatase. Finally, O$_2$ is reduced by those excited electrons to O$_2^\bullet$ while alcohol is oxidized to carbonyls (Fig. 4b).

In an analogous fashion, CeO$_2$ was also able to accommodate Au nanoparticles to realize the photocatalytic aerobic oxidation of alcohols to aldehydes in water under green LED irradiation (Scheme 4) [14]. The structure-function relationship between Au nanoparticle size and photocatalytic activity was probed. It was found that large-size Au nanoparticles prepared through multi-step photodeposition exhibited reaction rates nearly twice larger than small-size Au nanoparticles obtained by single-step photodeposition. The better activity of large-size Au/CeO$_2$ was attributed to its enhanced photo absorption. More interestingly, a high chemoselectivity toward alcohol oxidation was observed on the
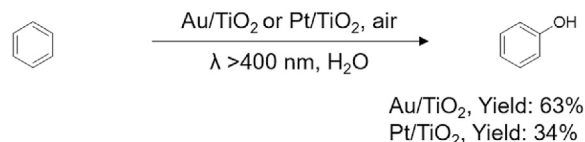
prepared Au/CeO$_2$. For example, aminobenzaldehyde was quantitatively generated from the oxidation of aminobenzyl alcohol using Au/CeO$_2$ as the photocatalyst (Scheme 4). Beyond alcohol oxidation, metal oxide semiconductors decorated with appropriate metal co-catalysts have been reported to facilitate many other organic transformations, such as benzene oxidation to phenol (Scheme 5) [15], amine oxidation to imine or aldehyde (Scheme 6) [16], and alkene epoxidation (Scheme 7) [17].

It has been demonstrated that heteroatoms (O, N, or S) are easily adsorbed on the surface of metal oxides and their energy levels of p orbitals are above the valence band of metal oxides, leading to new electron-donating sites. In addition, heteroatoms can be easily activated as they are normally electron rich atoms. Therefore, under the irradiation of visible light, there is electron transfer from heteroatoms to the conduction band of metal oxides (Fig. 5). The injected electrons can drive reductive reactions (*e.g.*, O$_2$ reduction) while the holes can drive organic oxidation transformations (Scheme 8 and 9) [18].
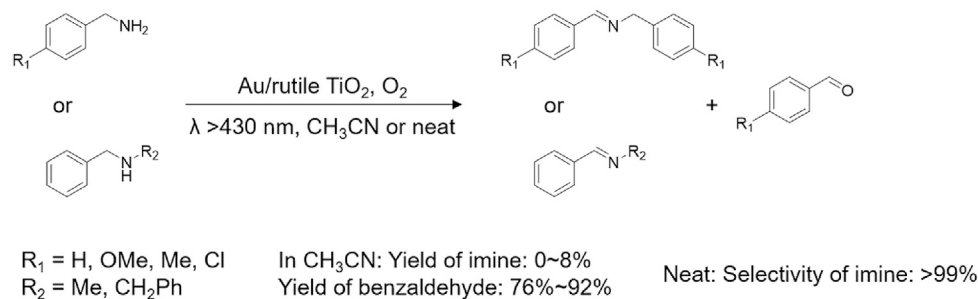
Unlike the other commonly used metal oxide semiconductors (*e.g.* TiO$_2$, ZnO, CeO$_2$), hematite (α-Fe$_2$O$_3$) is a promising visible light responsive semiconductor as it has a band gap of 2.2 eV and an
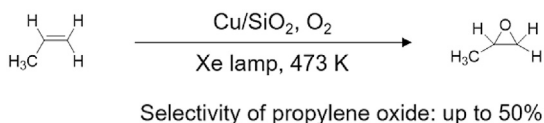

Yield: >99%

Scheme 4.

Au/TiO$_2$, Yield: 63%
Pt/TiO$_2$, Yield: 34%

Scheme 5.

R$_1$ = H, OMe, Me, Cl
R$_2$ = Me, CH$_2$Ph

In CH$_3$CN: Yield of imine: 0~8%
Yield of benzaldehyde: 76%~92%

Neat: Selectivity of imine: >99%

Scheme 6.

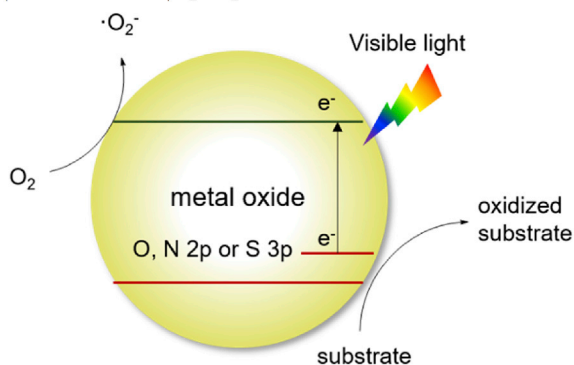Selectivity of propylene oxide: up to 50%

Scheme 7.

**Fig. 5.** Simplified band structure and reaction of a metal oxide decorated with heteroatoms.

appropriate valence band edge (2.5 V vs RHE) to drive oxidation reactions. However, it alone shows extremely poor activity for valuable oxidation reactions, such as organic sulfide oxidation and oxidative C—H activation. Several strategies have been developed to improve its property. Sun et al. reported a Ru(II)/α-Fe$_2$O$_3$ system for selective oxidation of benzyl alcohol and organic thioanisole. Their results indicate that the absorption of Ru(II) species plays a great role in the success of oxidation reactions [19]. Nearly 100% yield of sulfoxide and 5 times improvement in benzyl alcohol oxidation were obtained on Ru2/α-Fe$_2$O$_3$ photocatalyst compared to Ru1/α-Fe$_2$O$_3$, indicating the advantage of catalyst immobilization (Fig. 6). Wang et al. proposed a strategy for C—H activation of hydrocarbons on N-hydroxyphthalimide/α-Fe$_2$O$_3$ (NHPI/α-Fe$_2$O$_3$). The generated long-lived PINO* radical is essential for the success of C—H activation (Scheme 10) [20].

C—H bond activation can also be realized on bismuth-based oxides. For instance, Yuan et al. developed a surface-chlorinated BiOBr/TiO$_2$ photocatalyst for the selective activation of C(sp^3)-H bond under visible light irradiation (Scheme 11) [21]. Besides C—H activation, bismuth-based oxides (BiVO$_4$, Bi$_2$WO$_6$, Bi$_2$MoO$_6$) can also drive photocatalytic alcohol oxidation (Schemes 12—13) [22]. Compared to the well-established model reaction, benzyl alcohol oxidation, selective glycerol oxidation is a more challenging organic transformation owing to the co-existence of three reactive hydroxyl groups. Dihydroxyacetone is one of the oxidation products of glycerol which holds high value in industry. Xu et al. reported Bi$_2$WO$_6$ as a highly selective photocatalyst for the production of dihydroxyacetone from glycerol oxidation under ambient condition (visible light, in H$_2$O, room temperature, and atmospheric pressure). This work shows a promising application of bismuth-based photocatalysts for selective organic transformation (Scheme 14) [23].

2.2. Organic reductive transformations via metal oxide-based photocatalysts

Similar to photocatalytic oxidation reactions driven by excited holes (or resulting oxidizing species) on semiconductors, excited

R = H, Me, *t*-Bu, F, Cl, Br, NO$_2$

Yield: 52%~92%

Scheme 8.

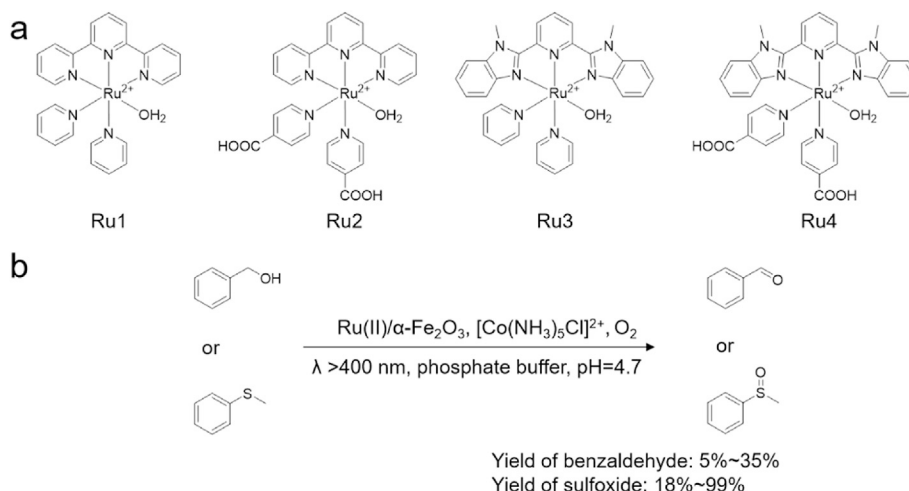R = H, Me, F, Cl

Yield: 32%~52%
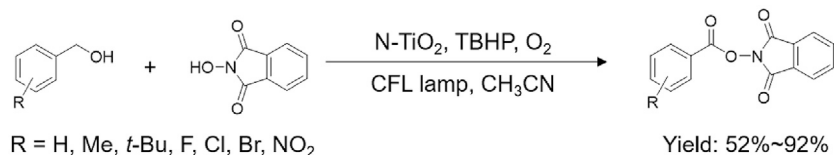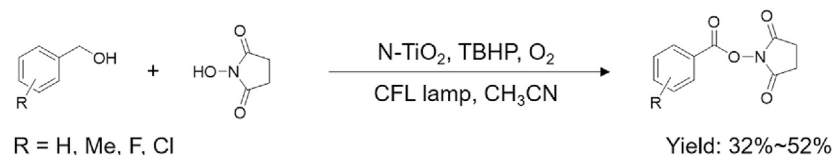
Scheme 9.

Fig. 6. (a) Molecular structures of ruthenium sensitizers. (b) Reaction schemes for the photocatalytic oxidation of benzyl alcohol and thioanisole.

electrons are able to perform the reductive transformations of organic compounds. For instance, Zhu et al. reported several metal oxide-based semiconductor photocatalysts (e.g., CeO₂, TiO₂, ZrO₂, Al₂O₃, and zeolite Y), for four reduction reactions, including nitro-aromatics to azo compounds, azobenzene hydrogenation to hydroazobenzene, ketone reduction to alcohols, and epoxide deoxygenation to alkenes [24]. Au nanoparticles were utilized as competent co-catalysts on metal oxide semiconductors, because of its strong visible light absorption resulting from the surface

plasmon resonance effect. A straightforward chemical reduction approach was employed to prepare Au nanoparticles on those semiconductors. Au nanoparticles with similar morphology were obtained with a homogeneous distribution on metal oxides and a nanoparticle size range of 5−8 nm (Fig. 7a). Their UV−vis diffuse reflectance spectra are compared in Fig. 7b and it is clear that all the five samples exhibit strong absorption in the visible range with a strong absorption peak at 520 nm, which is the characteristic feature of the surface plasmon resonance of Au nanoparticles.
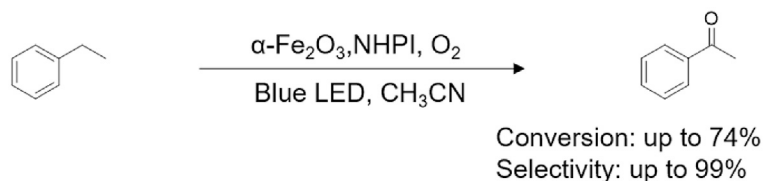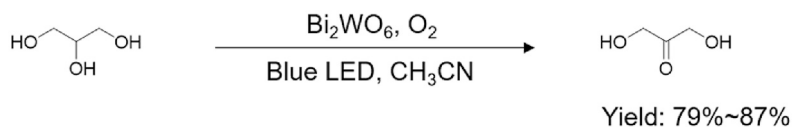

Scheme 10.
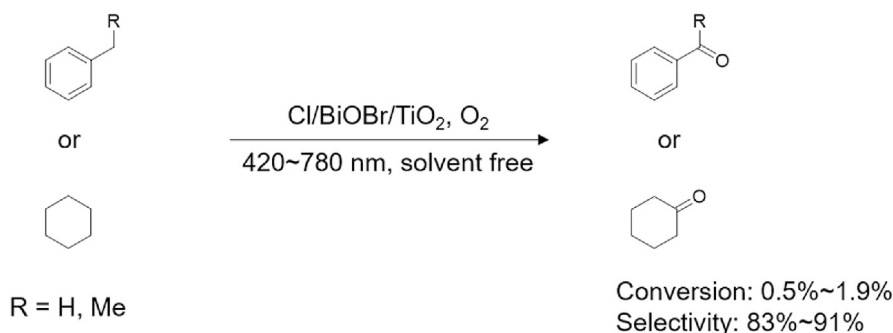
Scheme 11.
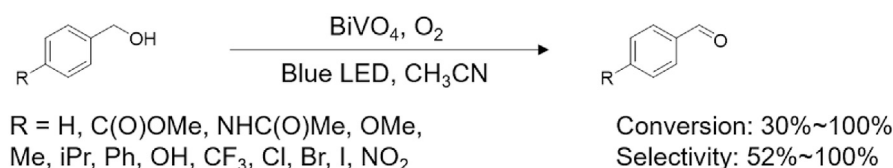
Scheme 12.
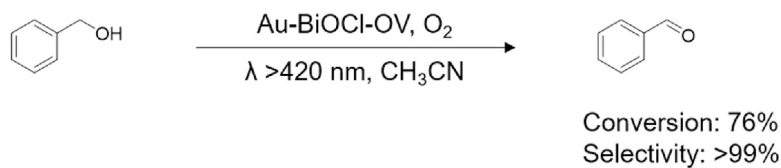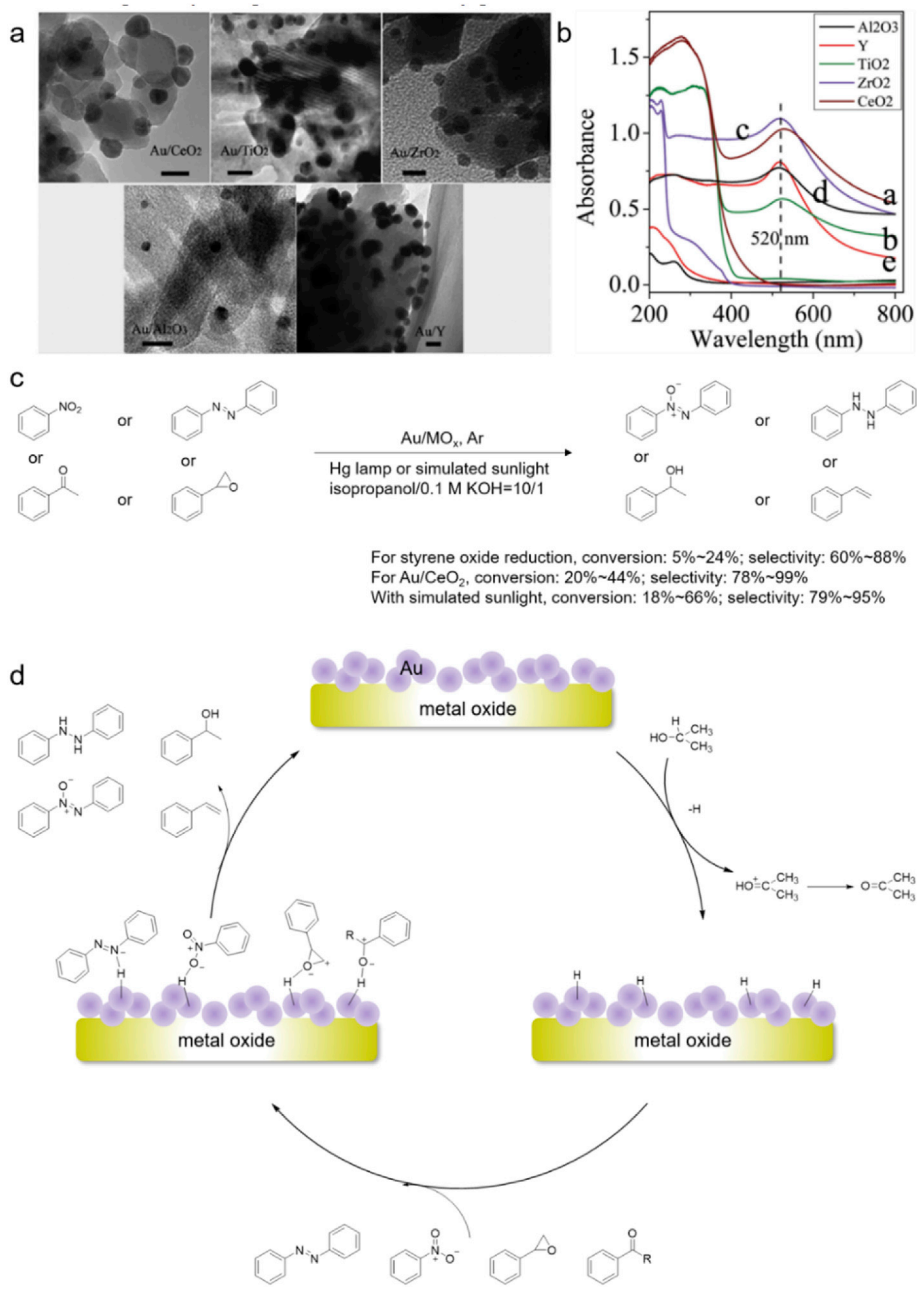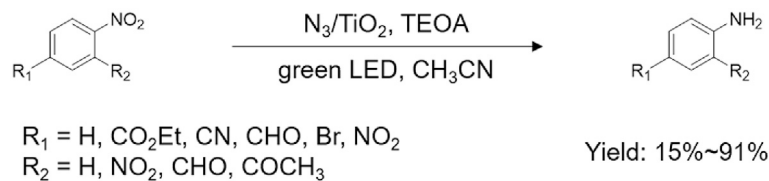
Scheme 13.

Scheme 14.

Fig. 7. (a) TEM images of Au nanoparticles on different supports (scale bar = 10 nm). (b) UV−vis diffuse reflectance spectra of Au nanoparticles on different supports. (c) Reaction pathways and (d) proposed mechanistic scheme for the photocatalytic reduction of various substrates on Au/MO$_x$.

R₁ = H, CO₂Et, CN, CHO, Br, NO₂
R₂ = H, NO₂, CHO, COCH₃

N₃/TiO₂, TEOA, green LED, CH₃CN

Yield: 15%~91%

Scheme 15.

Among these five semiconductors, only CeO_2 has absorption at wavelength longer than 500 nm while the other four counterparts only exhibit absorption at wavelength shorter than 400 nm. Consequently, it is anticipated that Au/CeO_2 may possess the best photocatalytic activity, which was confirmed through a model reaction − epoxide reduction in isopropanol/0.1 M KOH (v/v = 10/1). Under the same photocatalytic conditions, Au/CeO_2 was able to achieve the highest selectivity of styrene (88%) and relatively higher conversion (~20%) of epoxide. Furthermore, Au/CeO_2 was applied to drive other reduction reactions and it even exhibited excellent performance under simulated sunlight irradiation (Fig. 7c). A tentative mechanism was proposed and outlined in Fig. 7d. Isopropanol was employed as the proton source and adsorbed hydrogen was formed on Au nanoparticles during photocatalysis to yield $Au-H_{ads}$. $Au-H_{ads}$ was speculated to attack C=C or epoxide bonds and furnish hydrogen atom transfer, resulting in hydrogenation or deoxygenation reactions.

Reduction of nitrobenzene is a widely investigated organic reaction in photocatalysis [25]. The final reduction product of nitrobenzene is aniline [26] (Scheme 15), which is an important feedstock in chemical industry. Besides aniline, a series of intermediate compounds can also be generated through nitrobenzene reduction, such as nitrosobenzene, *N*-phenylhydroxylamine, azoxybenzene, azobenzene, and hydrazobenzene, among which azobenzene is widely used in the production of dyes, food additives, and pharmaceutical products [27]. Selectively photocatalytic nitrobenzene reduction to azobenzene has been intensively studied on various semiconductor-based photocatalytic systems. For example, Yuan et al. reported a novel Au doped CeO_2-based core-shell-satellite super-sandwich structure (o-CeO_2@SiO_2@c-CeO_2/Au) which exhibited unconventional luminescence and photocatalytic activity towards nitro-aromatics reduction to azo products under near-infrared (NIR) irradiation (Scheme 16) [28].

As both aniline and azobenzene have wide applications in industry, it is desirable to develop photocatalytic systems for the production of either aniline or azobenzene with high selectivity. Ebitani et al. synthesized Au nanoparticle-decorated Al_2O_3 (Au/Al_2O_3) with an average Au size of 3.9 ± 0.7 nm and a broad surface plasmon bond centered at 516.5 nm [29]. The prepared Au/Al_2O_3 exhibited a controllable photocatalytic production of either aniline or azobenzene from nitrobenzene reduction with extremely high yield (>95%) by simply changing the solvent environment. Formic acid facilitated the production of aniline and KOH in isopropanol could favor the generation of azobenzene (Fig. 8a). Mechanisms of
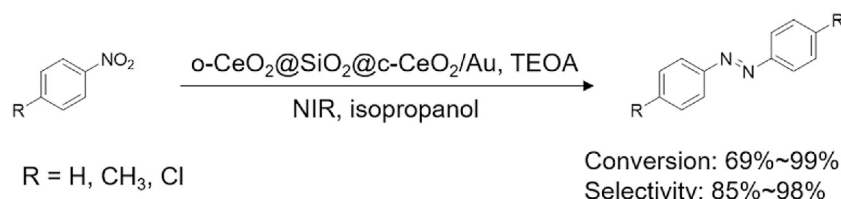
nitrobenzene reduction through both paths were proposed (Fig. 8b). In Path I, Au extracted protons from formic acid to form the active Au−H species followed by the transfer of hydrogen from Au−H to nitrobenzene resulting in H_2O elimination and aniline production. Step 2 was the rate-limiting step as nitrosobenzene was detected as the intermediate. In Path II, isopropanol was the hydrogen source and KOH facilitated the formation of alkoxide from isopropanol deprotonation. Following the release of H_2O and acetone, azobenzene could be formed. In this pathway, only azoxybenzene can be accumulated as the intermediate, proving that the condensation between nitrosobenzene and *N*-phenylhydroxylamine is fast and the last step from azoxybenzene to azobenzene is the rate-limiting step.

2.3. Redox-coupled reactions via metal oxide-based photocatalysts

Most photocatalytic organic syntheses only focus on one half-redox reaction, either oxidation or reduction. Therefore, it is inevitable to utilize excess hole/electron scavengers to furnish the redox cycle. However, in the presence of excess scavengers, the oxidation or reduction power of a photocatalyst is wasted and simultaneously by-products will be produced, rendering product separation and purification difficult. Therefore, following the principles of green chemistry, it is desirable to fully utilize both excited electrons and holes to generate value-added organic chemicals. In this part, we will introduce redox-coupled organic reactions achieved via metal oxide-based photocatalysts.

Bazyar et al. reported a nano Pd/ZnO photocatalyst for cross-coupling reactions, including Suzuki-Miyaura, Hiyama, and Buchwald-Hartwig reactions under visible light irradiation with high efficiency and selectivity (Scheme 17). According to several control experiments with different scavengers, the authors demonstrated the involvement of both excited electrons and holes in the reactions [30]. Besides Pd, the less expensive and easily prepared Ag-doped TiO_2 was also demonstrated as an efficient photocatalyst for Suzuki coupling under visible light irradiation (Scheme 18) [31]. Xiong et al. investigated the effect of oxide supports in Pd-oxide hybrid structure on the photocatalytic performance. The activity can be enhanced by a n-type semiconductor which will be reduced by a p-type semiconductor. Pd-tetra-TiO_2 exhibits the best performance in catalyzing the Heck reaction (Scheme 19) [32].

Pericàs et al. reported a cheap and non-toxic BiO_3 photocatalyst for an atom transfer radical addition (ATRA) reaction, which involves the simultaneous formation of C−Br and C−C bond through

R = H, CH₃, Cl

o-CeO_2@SiO_2@c-CeO_2/Au, TEOA, NIR, isopropanol

Conversion: 69%~99%
Selectivity: 85%~98%

Scheme 16.

a

Path I
Au/Al$_2$O$_3$, green LED
HCOOH, CH$_3$CN

Yield: 96%

Au/Al$_2$O$_3$, green LED
KOH, isopropanol
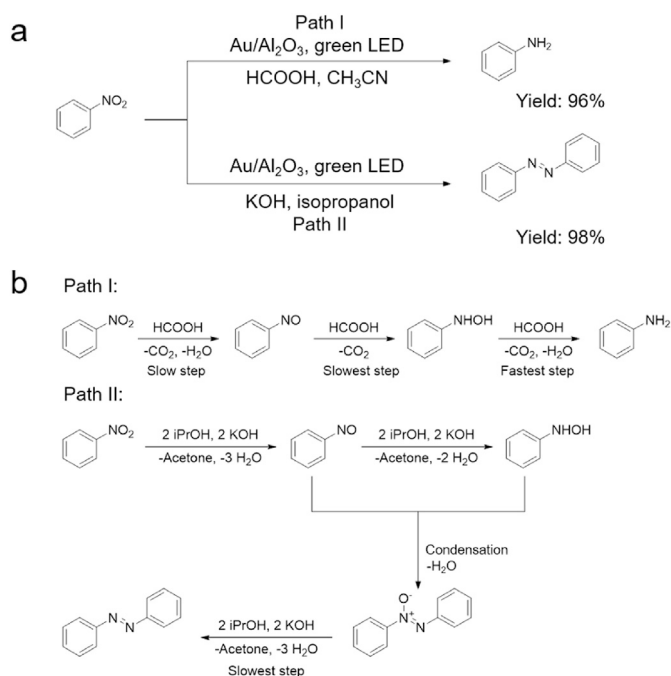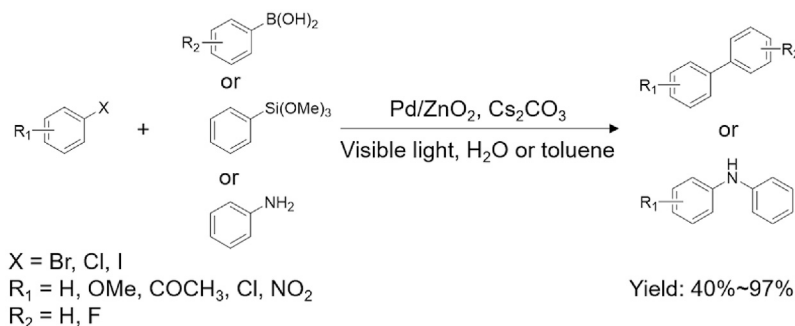Path II

Yield: 98%

b

Path I:

Path II:

Fig. 8. (a) Two reaction paths for the photocatalytic reduction of nitrobenzene. (b) Proposed reaction pathways for the reduction of nitrobenzene using either formic acid (Path I) or KOH and 2-propanol (Path II).

the addition of bromoalkenes across double bonds. The corresponding ATRA products are obtained with moderate to excellent
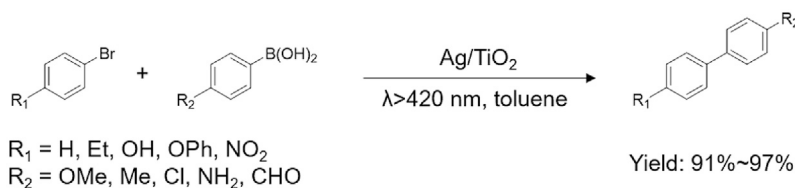
yield (Fig. 9a) [33]. A proposed mechanism was shown in Fig. 9b, the excited electrons can cleave the C—Br bond to generate radical I. Subsequently, radical I undergoes addition to the double bond of olefin, giving raise to the radical intermediate II. Then, there are two possible pathways: a radical-polar crossover (path a) and a radical chain propagation (path b). In path a, radical II is oxidized by the excited holes to a carbocation III, which further reacts with bromide, forming the ATRA product. In path b, radical I abstracts a bromine atom from the starting compound to form the desired product and the regenerated radical I can continue the chain.

3. Photocatalytic reactions of organic compounds on metal sulfide/selenide semiconductors
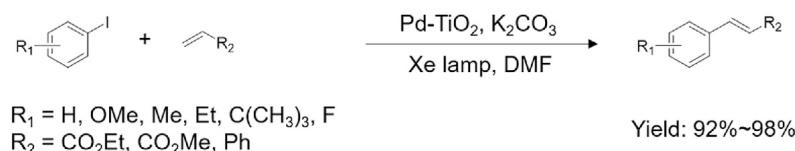
Besides metal oxide, metal sulfide/selenide is another major class of semiconductors for photocatalytic organic transformations. Compared to metal oxides, metal sulfides/selenides have smaller band gaps, enabling better visible light absorption. For example, CdS has a band gap of 2.4 eV, therefore it can absorb light up to 520 nm. To date, numerous reports have been published in photocatalytic organic transformations utilizing metal sulfide/selenide semiconductors, including both oxidation reactions (e.g., selective oxidation of alcohols and amines, as well as oxidative C—C coupling), reduction reactions (e.g., selective reduction of nitrobenzene, cyclization, and reductive C—C coupling), and redox-coupled reactions (e.g., benzyl alcohol oxidation coupled with nitrobenzene reduction). In this section, we will summarize the recent advance in photocatalytic organic transformations based on metal sulfide/selenide photocatalysts.

X = Br, Cl, I
R$_1$ = H, OMe, COCH$_3$, Cl, NO$_2$
R$_2$ = H, F

Pd/ZnO$_2$, Cs$_2$CO$_3$
Visible light, H$_2$O or toluene

Yield: 40%~97%

Scheme 17.

R$_1$ = H, Et, OH, OPh, NO$_2$
R$_2$ = OMe, Me, Cl, NH$_2$, CHO

Ag/TiO$_2$
λ>420 nm, toluene

Yield: 91%~97%

Scheme 18.

R$_1$ = H, OMe, Me, Et, C(CH$_3$)$_3$, F
R$_2$ = CO$_2$Et, CO$_2$Me, Ph

Pd-TiO$_2$, K$_2$CO$_3$
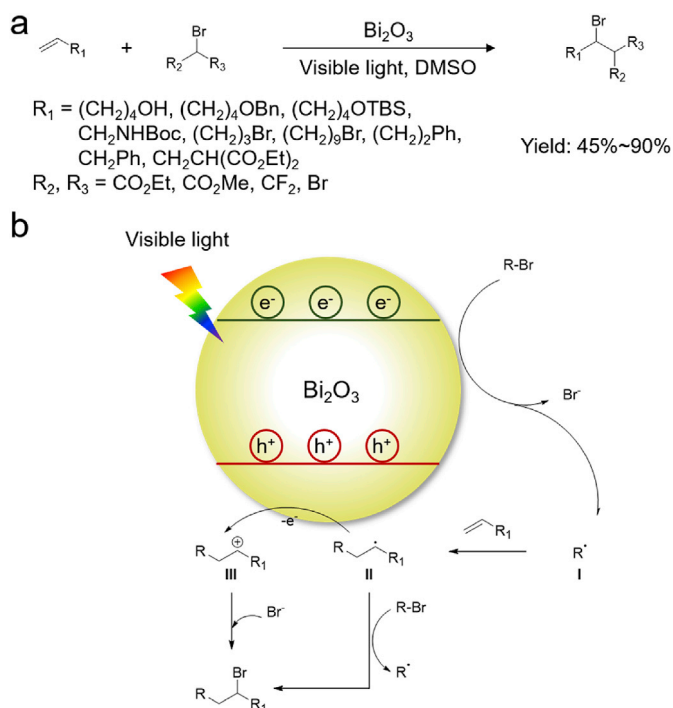Xe lamp, DMF

Yield: 92%~98%

Scheme 19.

Fig. 9. (a) Reaction pathways and (b) proposed mechanistic scheme for the photocatalytic atom transfer radical addition reaction.

3.1. Organic oxidative transformations via metal sulfide/selenide-based photocatalysts

Alcohol oxidation is one of the most investigated model reactions. However, the selective oxidation of alcohols is still a challenging task, especially when multiple hydroxyl groups are available in complex natural products. Fig. 10a shows three examples of polyhydroxy natural products. Wu et al. reported a photocatalyst consisting of 3-mercaptopropionic acid (MPA)-capped CdSe quantum dots (MPA-CdSe QDs), which exhibited excellent photocatalytic activity for the selective oxidation of alcohols (Fig. 10b) [34]. Not only primary and secondary aromatic alcohols were oxidized to their corresponding aldehydes/ketones, but also aliphatic alcohols could be oxidized with a moderate conversion and selectivity. Moreover, MPA-CdSe QDs-Ni^{2+} demonstrated great potential for site-selective alcohol oxidation of polyhydroxy natural products. For example, Estradiol related compound C was produced with a high yield of 70% on a gram scale. The reaction mechanism is speculated in Fig. 10c. Upon light irradiation, the excited holes oxidize the adsorbed thiolate anions to thiyl radicals, which can abstract hydrogens from benzyl alcohol to produce benzylic radicals and lead to the formation of benzaldehyde. In the meantime, the abstracted hydrogens are reduced by excited electrons to produce H$_2$ on Ni.

Besides CdSe, various other metal sulfides/selenides are also proved to be efficient photocatalysts for alcohol oxidation [35]. Xie et al. prepared cubic In$_2$S$_3$ nanosheets with S vacancies through a hydrothermal method. Both S vacancy-rich and -poor samples were synthesized and theoretical calculation demonstrated that the introduction of S vacancies led to enhanced charge separation and transfer. Hence, for photocatalytic alcohol oxidation, the aldehyde yield on S vacancy-rich In$_2$S$_3$ was ca. 2-fold higher compared to that achieved on the S vacancy-poor In$_2$S$_3$ photocatalyst (Scheme 20) [36]. Bartlett et al. reported nitrate-mediated alcohol oxidation on CdS [37]. They showed that nitrate could act as a mediator and enhance the photocatalytic activity greatly. Nitrate-mediated CdS

achieved an excellent benzaldehyde yield (70%–100%) from benzyl alcohol oxidation with a rate up to 13.6 mM h^{-1}, compared to 8% yield at 3 mM h^{-1} without nitrate mediator. More importantly, this catalyst could also drive the oxidation of 5-hydroxymethylfurfural (HMF) to 2,5-diformylfuran (DFF) with a rate of 2.6 mM h^{-1} (Scheme 21).

It should be noted that HMF upgrading holds a vital role in biomass refinery as HMF is one of the top biomass-derived platform compounds which could be used for the production of a great variety of value-added chemicals. The Sun group reported that ultrathin Ni/CdS with a thickness around 1.1 nm (Fig. 11a and b) could act as a competent photocatalyst for the oxidation of biomass-derived alcohols [38]. Nearly quantitative amount of furfural was produced from furfural alcohol on Ni/CdS under visible light irradiation. However, under the same condition, the DFF yield (20%) from HMF oxidation was much lower, which may be caused by the slightly stronger binding affinity of the aldehyde group relative to the alcohol group in HMF toward Ni/CdS. Nevertheless, under alkaline condition, another highly valuable product, 2,5-furandicarboxylic acid (FDCA) could be formed from HMF oxidation with a yield higher than 90% using Ni/CdS (Fig. 11c). Overall, these results demonstrate that one could selectively produce either aldehydes or carboxylates via readily tuning the photocatalysis solvent.

Up to now, only quite low yield of DFF (<40%) could be realized utilizing most heterogeneous photocatalysts, including not only metal sulfides/selenides but also other semiconductors like metal oxides and carbon-based materials [39]. To the best of our knowledge, the highest DFF yield ever reported was ~71% (Scheme 22), wherein a Z-scheme ZnIn$_2$S$_4$/Nb$_2$O$_5$ photocatalyst was employed and the Z-scheme heterostructure was proposed to be a key factor for the high photocatalytic activity [40].

Another type of important organics obtained from alcohol oxidation is C–C coupling products. The first example of visible light-driven photocatalytic synthesis of C–C coupling products, hydrobenzoin and benzoin, from benzyl alcohol oxidation on CdS was reported by König et al. [41], even though a mixture of benzaldehyde and C–C coupling products (hydrobenzoin and benzoin) were obtained (Scheme 23). It would be more desirable to produce either benzaldehyde or C–C coupling products with high selectivity. Weiss et al. achieved this goal via utilizing visible light-absorbing CdS quantum dots (QDs) and their system could drive the photocatalytic benzyl alcohol oxidation to either benzaldehyde or C–C coupling products (mainly hydrobenzoin) with over 91% selectivity by controlling the photodeposited Cd(0) species (Fig. 12a) [42]. A proposed mechanism is sketched in Fig. 12b. Benzyl alcohol was oxidized by the excited holes to generate a ketyl radical intermediate, followed by further oxidation to benzaldehyde. In the presence of Cd(0), a back reduction from benzaldehyde to ketyl radical would take place, leading to C–C coupling products. Another strategy to control the selectivity of benzyl alcohol oxidation was reported by Wang et al. They tuned the conduction band position of zinc indium sulfide by changing the atomic ratio between Zn and In. Through this approach, either deoxybenzoin (yield: 61%) or benzoin (yield: 64%) could be generated as the major product (Scheme 24) [43]. In addition, the high selectivity of benzoin or deoxybenzoin could also be obtained by fine tuning the photocatalytic conditions (Scheme 25) [44].

Besides C–C coupling reactions, C-X coupling is also significant in organic synthesis, in which oxidative coupling of amine to imine is a representative reaction. A generally accepted mechanism is shown in Fig. 13. Upon light irradiation, the excited holes oxidize benzylamine to the corresponding radical cation. Meanwhile, the excited electrons reduce O$_2$ to superoxide radical anion, which reacts with the amine radical cation to form the intermediate
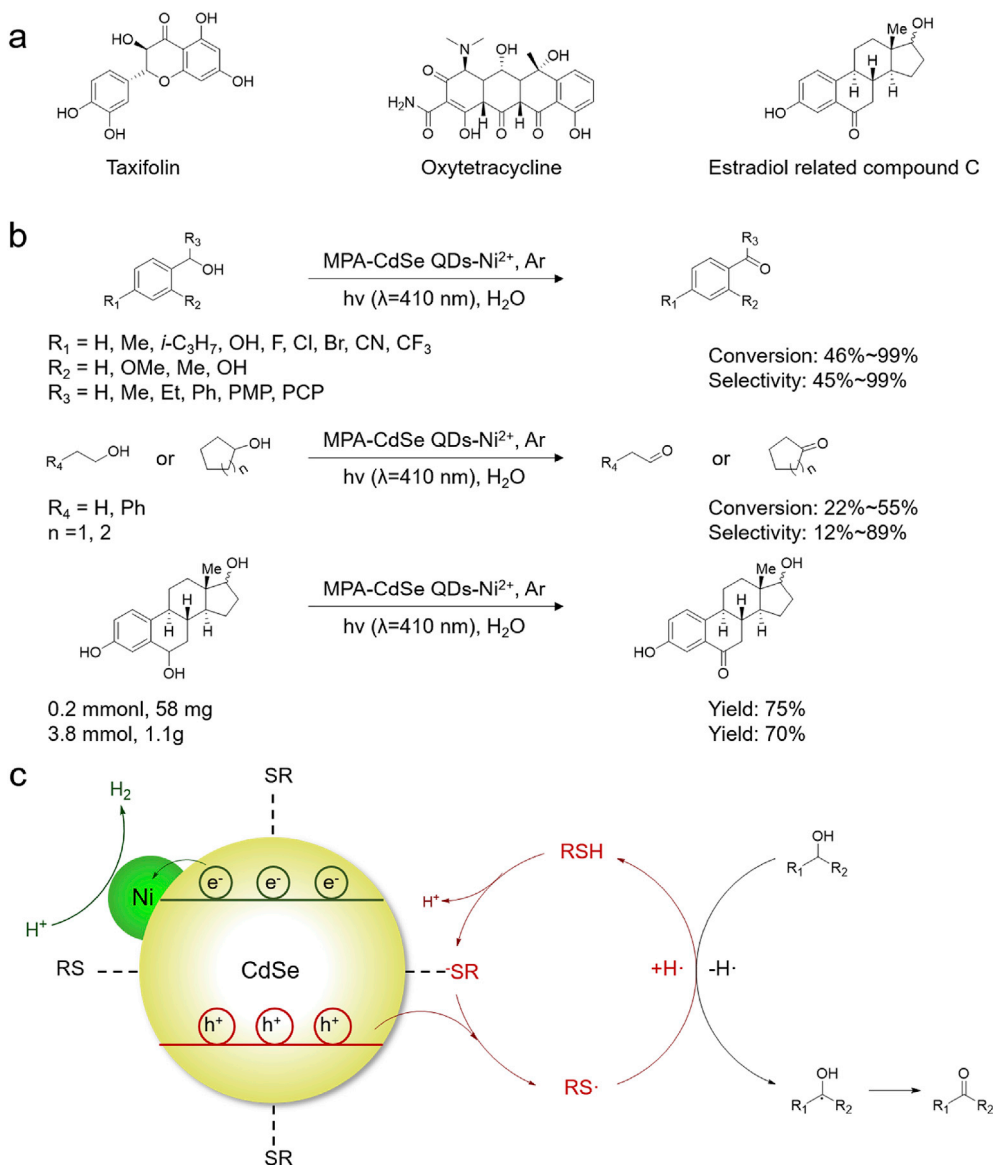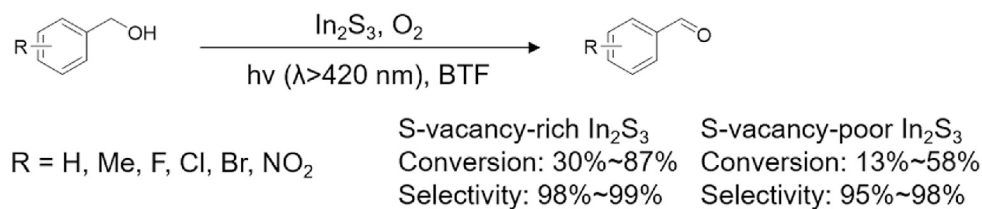
Fig. 10. (a) Representative examples of polyhydroxy natural products. (b) Selective photocatalytic oxidation of alcohols on MPA-CdSe with QDs-Ni^{2+}. (c) Proposed reaction mechanism for the photocatalytic oxidation of alcohols on MPA-CdSe with QDs-Ni^{2+}.
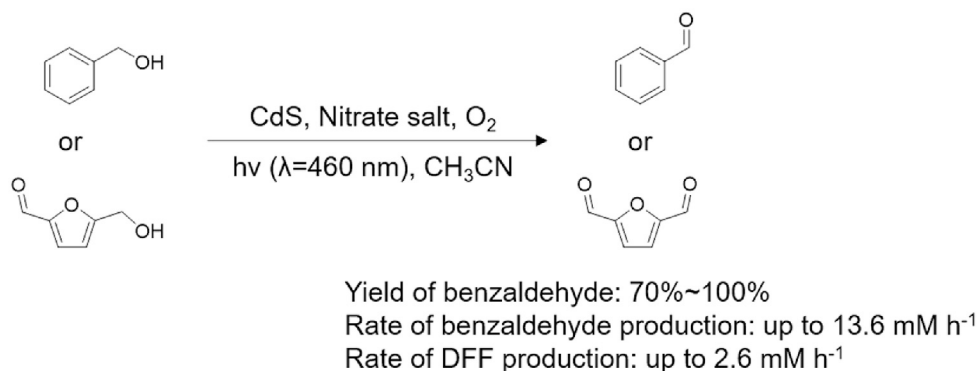

Scheme 20.

imine. After the addition of another amine and removal of ammonia, the coupling product is produced. During this process, benzaldehyde was detected as an intermediate, suggesting that the decomposition of peroxide may hydrolyze the imine intermediate to aldehyde, which combines with another amine to form the coupling product. Several metal sulfides have been proved to act as efficient photocatalysts for C—N coupling of benzylamine, such as monolayer WS$_2$ nanosheets (Scheme 26) [45], CdS nanowires

(Scheme 27) [46], ZnIn$_2$S$_4$ nanospheres (Scheme 28) [47], and MoS$_2$ nanosheets (Scheme 29) [48].

3.2. Organic reductive transformations via metal sulfide/selenide-based photocatalysts

König et al. reported a photocatalytic approach for reductive dehalogenation and C—H arylation reactions through the
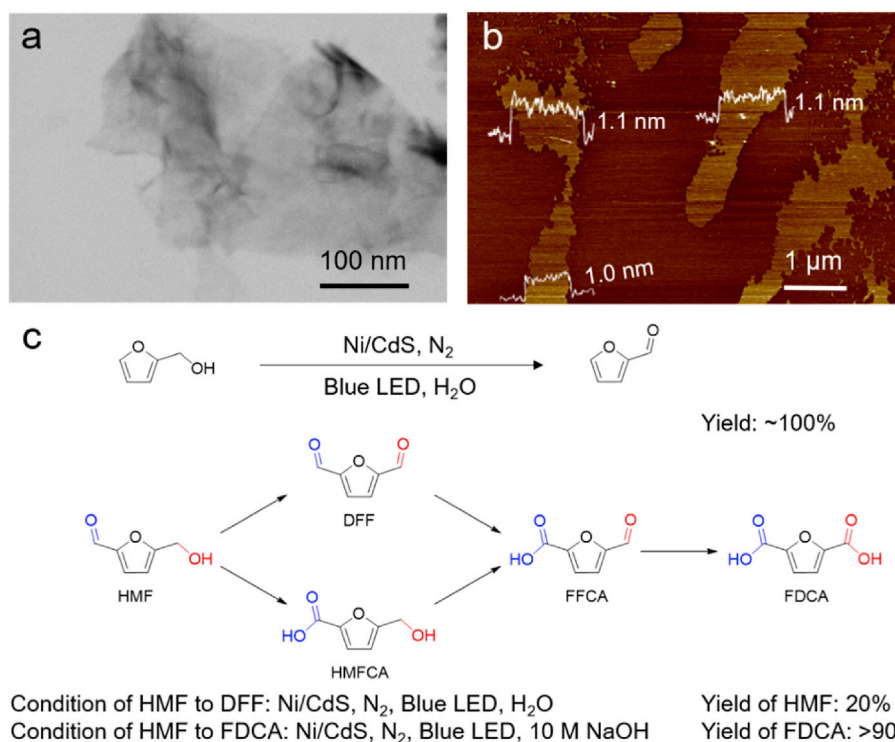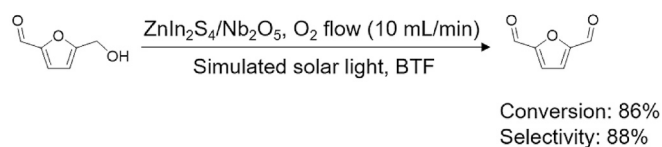
Scheme 21.

Yield of benzaldehyde: 70%~100%
Rate of benzaldehyde production: up to 13.6 mM h^{-1}
Rate of DFF production: up to 2.6 mM h^{-1}

Fig. 11. (a) TEM and (b) AFM images of ultrathin Ni/CdS. (c) Reaction pathways for the oxidation of furfural alcohol and HMF.

Conversion: 86%
Selectivity: 88%

Scheme 22.

generation of highly active (hetero)aryl radicals from their corresponding halides [49]. Traditionally, the generation of aryl radicals from aryl halides is always challenging owing to the extremely high reduction potential, hence strong base or nucleophile is always needed. In this work, they overcame this challenge by applying ZnSe/CdS core-shell QDs as the photocatalyst. Because of the high surface area, homogeneity, and high stability, the prepared ZnSe/CdS QDs exhibited outstanding photocatalytic activity for dehalogenation and C−H arylation reactions under mild condition

(Fig. 14a). The proposed photocatalytic mechanism is depicted in Fig. 14b. Upon visible light irradiation, the produced excited holes oxidize N,N-diisopropylethylamine (DIPEA) to a radical cation while the excited electrons drive the reduction of aryl halide to its corresponding radical anion, which releases a halide ion to become a neutral radical. Subsequently, the aryl radical can be trapped by a pyrrole compound to yield the desirable C−H arylated products or extract a hydrogen atom from DIPEA to generate the dehalogenated reduction product. Photocatalytic reductive dehalogenation has also been reported by Weix et al. utilizing CdSe QDs as the photocatalyst (Scheme 30) [50]. In fact, the reaction scope could be expanded to β-alkylation, β-aminoalkylation, amine arylation, and decarboxylative radical addition to styrene.

Because of the advantageous properties of QDs such as visible-light-harvesting capability, tunable redox potential, and large surface area, metal sulfide/selenide QDs have gained increasing popularity in photocatalytic organic reduction. For example, the reductive synthesis of amines from imines was realized using CdSe/
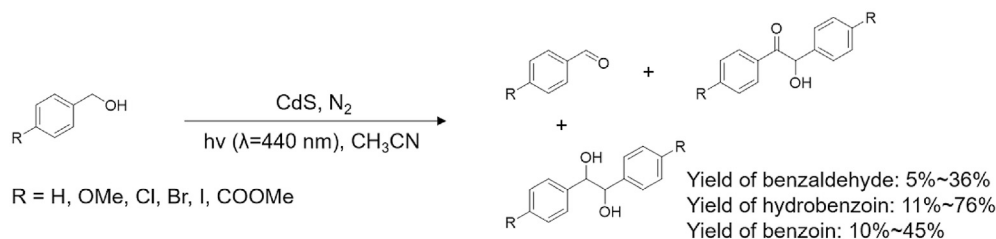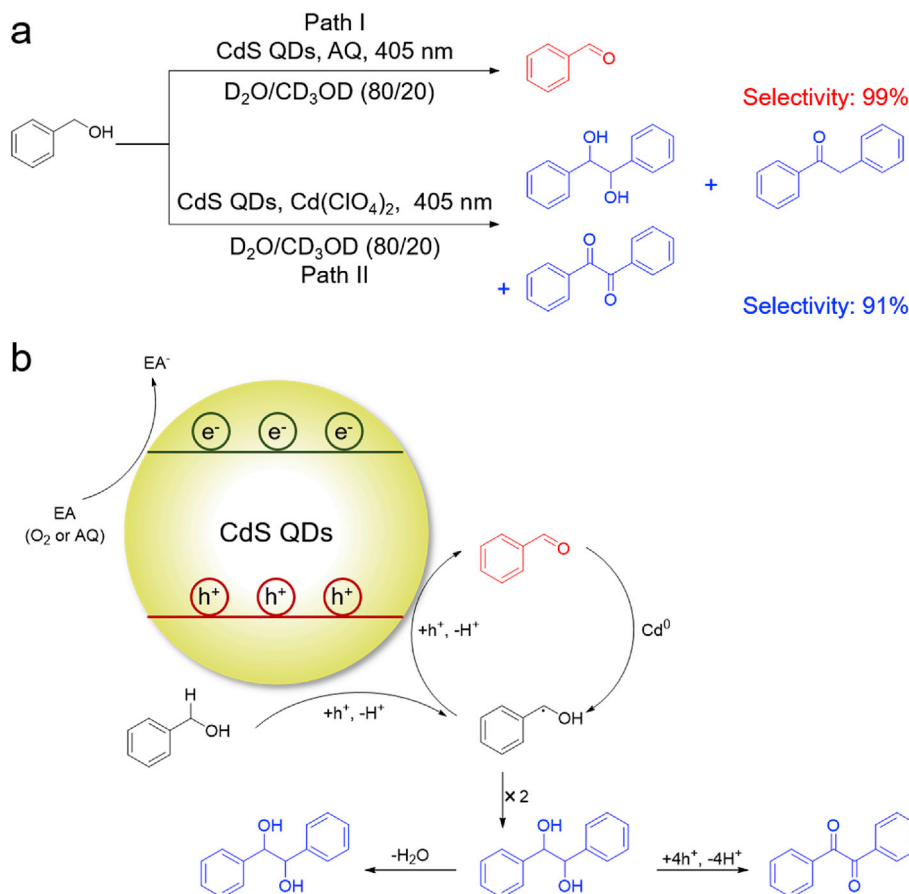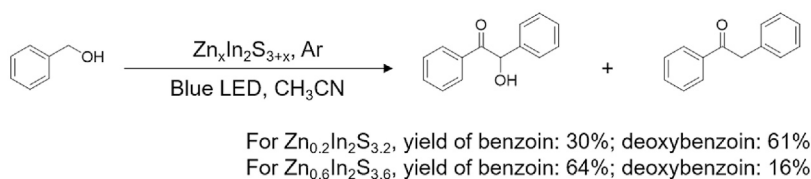
Scheme 23.

Fig. 12. (a) Photocatalytic pathways of benzyl alcohol oxidation to either benzaldehyde or C−C coupling products; (b) Proposed mechanism for the photocatalytic oxidation of benzyl alcohol.


For $Zn_{0.2}In_2S_{3.2}$, yield of benzoin: 30%; deoxybenzoin: 61%
For $Zn_{0.6}In_2S_{3.6}$, yield of benzoin: 64%; deoxybenzoin: 16%

Scheme 24.

CdS core/shell QDs as the photocatalyst and thiophenol as a hydrogen atom donor [51]. A wide range of aromatic amines with different substituents were obtained with excellent yields (Scheme 31). Moreover, a direct one-pot reaction between amine and aldehyde proceed smoothly to give hetero-coupling amine with excellent yields (66%−93%, Scheme 32). Furthermore, a biologically active amine, butenafine could be synthesized following this approach with a yield of 65%, manifesting the promise of CdSe/CdS core/shell QDs photocatalyst in the green synthesis of

pharmaceuticals (Scheme 33).

Recently, Weiss et al. employed CdSe QDs in alkene cycloaddition reactions with extremely high diastereoselectivity and regioselectivity [52]. Fig. 15a shows the reaction activity and diastereoselectivity, wherein CdS QDs generate syn products with a diastereoselective ratio (d.r.) > 30:1. Not only homo-coupling products but also hetero-coupling products (compound **2** reacted with **1** or **3**) could be efficiently formed with d.r. > 40:1 and a yield up to 92%. The regioselectivity of this reaction can be tuned through
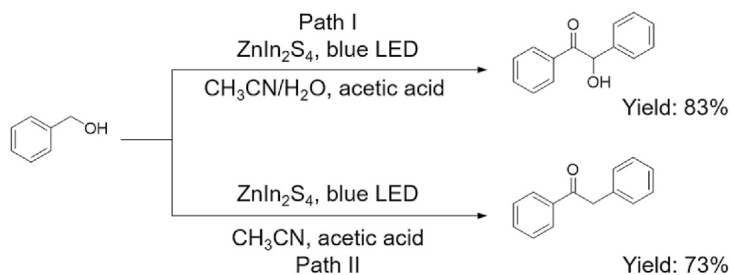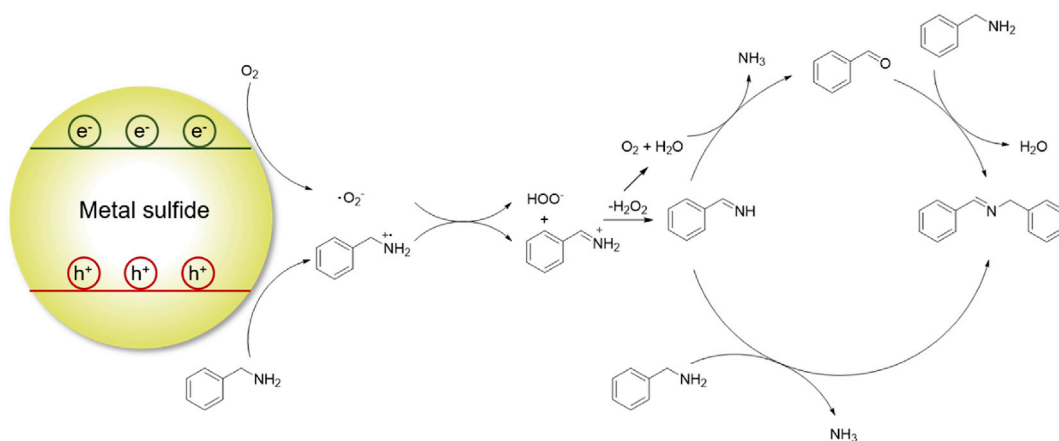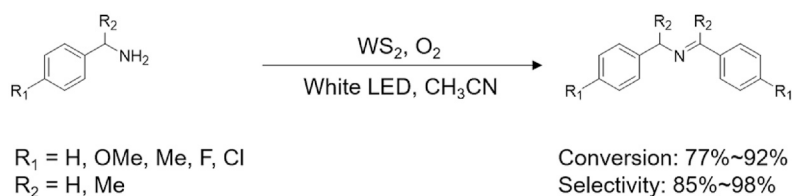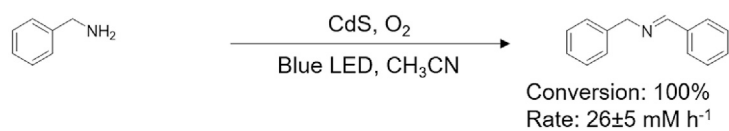
Scheme 25.

Fig. 13. Proposed mechanism for the photocatalytic oxidation of benzyl amine.

R₁ = H, OMe, Me, F, Cl
R₂ = H, Me

Conversion: 77%~92%
Selectivity: 85%~98%

Scheme 26.

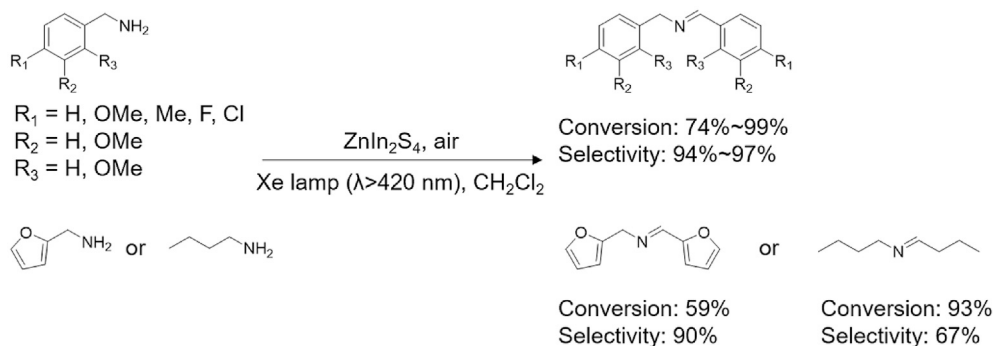Conversion: 100%
Rate: 26±5 mM h⁻¹

Scheme 27.

the position of the carboxylate moiety, *e.g.* **4** versus **5**, and **6** versus **7**. For the coupling of **4** and **2**, a nearly perfect head-to-head (HH) regioisomer was obtained. However, the coupling between **5** and **2** completely switched the regioselectivity to yield a head-to-tail (HT) product with regioselective ratio (r.r.) > 40:1 (Fig. 15b).
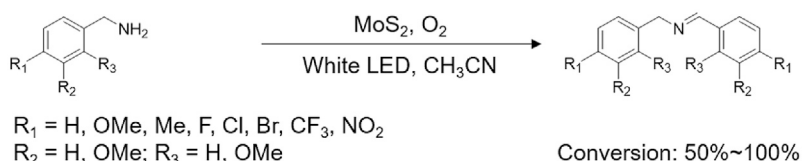
3.3. Redox-coupled reactions via metal sulfide/selenide-based photocatalysts

Selective benzyl alcohol oxidation and nitrobenzene reduction are two representative model reactions. Numerous works of each individual reactions have been reported, however, the integration of these two reactions in one photocatalytic system is rare. Chen et al. reported that benzaldehyde and benzyl amine (or nitrosobenzene) could be produced simultaneously in a one-pot system without any sacrificial reagents [53]. Through this process, both of the excited holes and electrons are utilized and two valuable industry feedstocks are produced with moderate to excellent yields (Scheme 34). The same group also reported the dehydrogenation and hydrogenolysis of benzyl alcohol to benzaldehyde and toluene simultaneously [54]. The combined yields of benzaldehyde and toluene were up to 94% (Scheme 35). In this system, the two half reactions can be coupled together with high yields because the dehydrogenation of alcohol consumes two holes and generates two protons while the hydrogenolysis reaction consumes two electrons and two protons.

R$_1$ = H, OMe, Me, F, Cl
R$_2$ = H, OMe
R$_3$ = H, OMe

ZnIn$_2$S$_4$, air
Xe lamp (λ>420 nm), CH$_2$Cl$_2$

Conversion: 74%~99%
Selectivity: 94%~97%

Conversion: 59%
Selectivity: 90%

Conversion: 93%
Selectivity: 67%

Scheme 28.

R$_1$ = H, OMe, Me, F, Cl, Br, CF$_3$, NO$_2$
R$_2$ = H, OMe; R$_3$ = H, OMe

MoS$_2$, O$_2$
White LED, CH$_3$CN

Conversion: 50%~100%

Scheme 29.

a

X = Br, Cl; Y = H, N
R$_1$ = CN, Cl, Br, CF$_3$, COOCH$_3$
R$_2$ = H, CN

ZnSe/CdS QDs, DIPEA
455 nm, hexane

Yield: 23%~92%

b

Visible light

ZnSe/CdS QDs

DIPEA

DIPEA$^{\cdot+}$

Ar-X

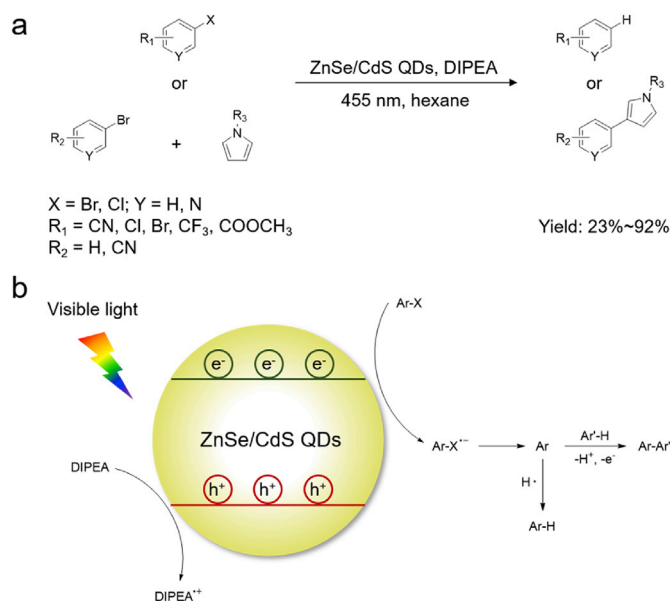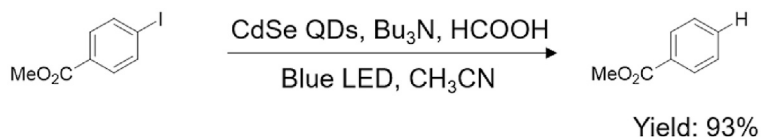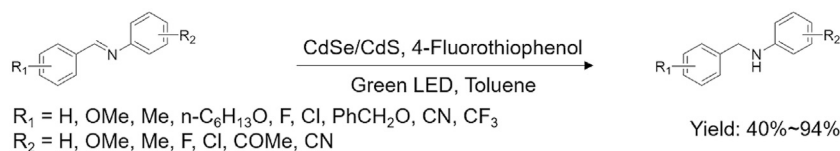Ar-X$^{\cdot-}$ → Ar $\xrightarrow[-H^+, -e^-]{Ar'-H}$ Ar-Ar'

H·

Ar-H

Fig. 14. (a) Photocatalytic paths of reductive dehalogenation and C−H arylation. (b) Proposed mechanism of photocatalytic dehalogenation and C−H arylation.

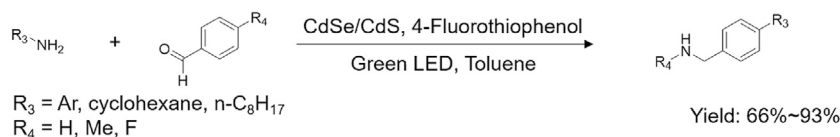CdSe QDs, Bu$_3$N, HCOOH
Blue LED, CH$_3$CN

Yield: 93%

Scheme 30.

Besides benzyl alcohol, other substrates which can be easily oxidized to value-added chemicals are also worth acting as candidates to couple with the reduction of nitrobenzene. Han et al. reported such a coupling system, wherein arabinose and azobenzene were produced simultaneously from glucose oxidation and nitrosobenzene reduction [55]. Arab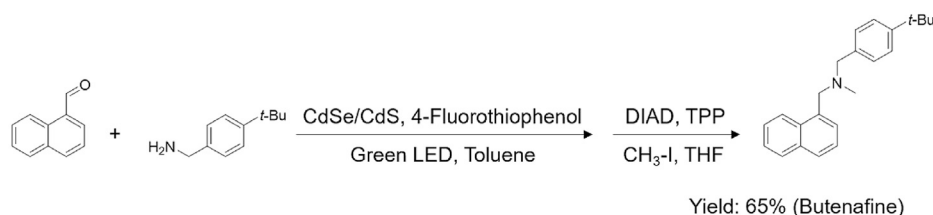inose is an important chemical in the pharmaceutical synthesis. Traditionally, it is synthesized from the derivatives obtained from glucose. In this work, the direct transformation from glucose to arabinose is quite appealing. More importantly, a high selectivity of arabinose (70%) was obtained, accompanying with a high selectivity of azoxybenzene (92%) (Scheme 36).

R_1 = H, OMe, Me, n-C_6H_13O, F, Cl, PhCH_2O, CN, CF_3
R_2 = H, OMe, Me, F, Cl, COMe, CN

Yield: 40%~94%

Scheme 31.

R_3 = Ar, cyclohexane, n-C_8H_17
R_4 = H, Me, F

Yield: 66%~93%

Scheme 32.

Yield: 65% (Butenafine)

Scheme 33.

C–C coupling reactions hold a pivotal role in the synthesis of various value-added chemicals, especially from cheap and abundant feedstocks like methanol. An interesting work utilizing methanol as a C1 carbon source is the hydrofunctionalization of olefins on CdS under visible light irradiation [56]. A wide range of aliphatic olefins were successfully hydrofunctionalized to higher aliphatic alcohols with great selectivity. In addition, not only methanol but also acetone and acetonitrile can also couple with olefins to produce industrially important chemicals (Scheme 37).

Suzuki C–C coupling, a noble-prize reaction, involves redox processes (oxidative addition and reductive elimination), which can be triggered by a photocatalyst. The excited holes are essential for activating arylboronic acids by cleaving the C–B bonds and the excited electrons can help to reduce aryl halides into aryl radicals. Pd-based catalysts, including organometallic homogeneous Pd complex and heterogeneous Pd nanoparticles on solid supports, are generally regarded as efficient catalysts for Suzuki coupling. Therefore, several photocatalytic systems combining Pd nanoparticles and semiconductors have been developed, including Pd/WS_2 (Scheme 38) [57], and Pd/MoS_2 (Scheme 39) [58], all of which exhibited moderate to decent reaction yields.

Lignin is one of the most abundant biomass materials, which is a highly functionalized biopolymer that has great potential for the production of small aromatics. The cleavage of the β-O-4 linkage in lignin has been regarded as an effective strategy in the depolymerization of recalcitrant lignin. A two-step pathway for β-O-4 cleavage has been proposed: C_α-OH oxidation followed by reductive bond breaking. The 1st oxidation step is initiated by excited holes while the following step is facilitated by excited electrons. Wang et al. reported CdS QDs as a photocatalyst for the photocleavage of a lignin model compound with excellent yield (Fig. 16a) [59]. More importantly, their approach can be applied in the fraction and valorization of native lignin as well. Theoretical calculations indicate that the energy of oxidative dehydrogenation of C_α-H in the lignin model compound is the least positive, which means C_α-H is the easiest bond to be broken by excited holes. In addition,

the excited electrons of CdS QDs have enough energy to perform the following reductive bond cleavage step (Fig. 16b). Besides CdS QDs, other photocatalysts also show a great potential for the valorization of lignin, e.g. Ni/CdS nanosheets (Scheme 40) [60] and ZnIn_2S_4 nanosheets (Scheme 41) [61].

4. Photocatalytic reactions of organic compounds on carbon nitride semiconductors

Although metal sulfides/selenides are effective visible-light-harvesting photocatalysts, their potential corrosive nature could limit their long-term application. In contrast, carbon nitride (CN) consisting of only light elements has emerged as a more promising photocatalyst thanks to its visible-light responsive feature (band gap of 2.7 eV), excellent thermal and chemical stability, and benign metal-free components. More importantly, its redox properties can be easily tuned by doping or morphology modification, which enables a fine modulation of its photocatalytic activity.

4.1. Organic oxidative transformations via carbon nitride-based photocatalysts

Selective oxidation of benzyl alcohol to benzaldehyde is a fundamental reaction in chemical industry. Wang et al. reported photocatalytic benzyl alcohol oxidation to benzaldehyde utilizing graphitic carbon nitride (g-CN) as the photocatalyst [62]. If bulk g-CN was employed, the conversion of benzyl alcohol was extremely low (~5%) due to the small surface area (~8 m^2/g) of bulk g-CN. Once a hard template method was adopted to synthesize mesoporous graphitic carbon nitride (mpg-CN) with a high surface area of ~200 m^2/g, a much higher benzylaldeyde yield of 57% was obtained under the same condition (Fig. 17a). A radical mechanism was proposed in Fig. 17b. The excited electrons reduce O_2 to superoxide radical anion ($\cdot O_2^-$), which deprotonated the alcohol substrate to form an alkoxide anion. Subsequent oxidation of the alkoxide anion by the excited holes yielded a radical and another hydrogen atom
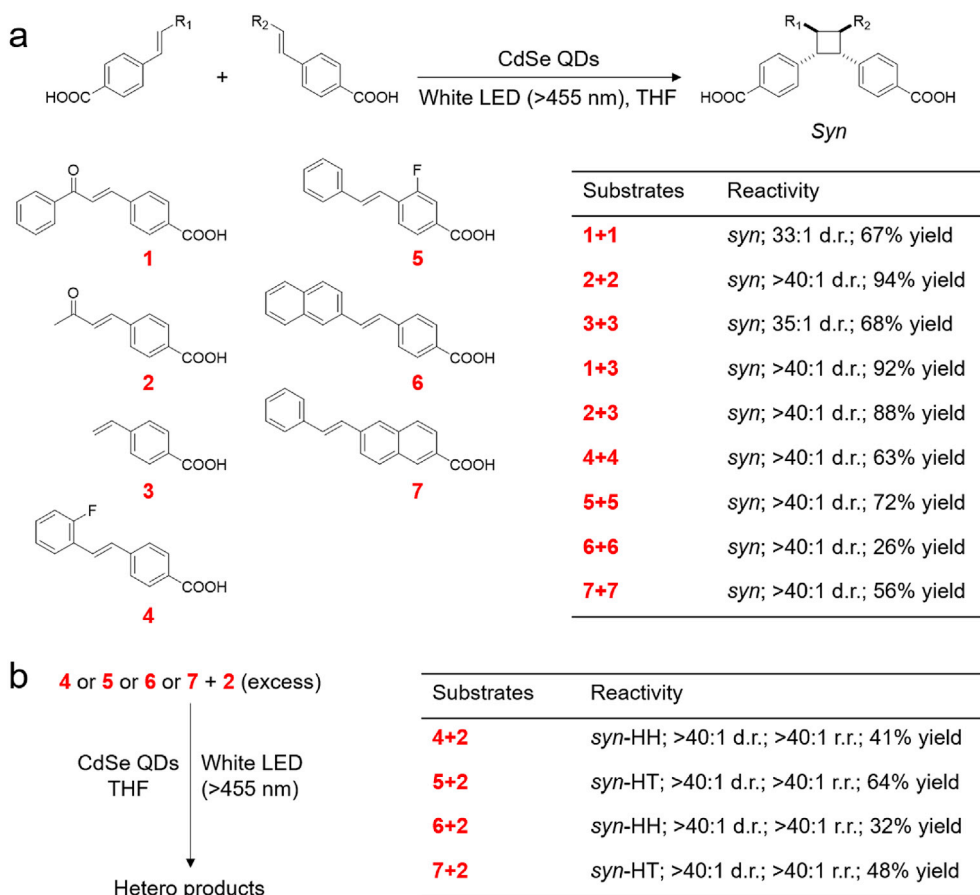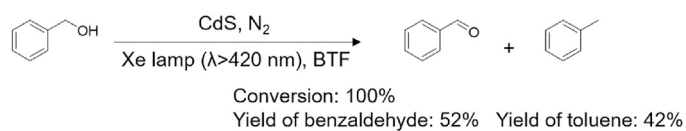
Fig. 15. (a) Diastereoselective intermolecular [2 + 2] cycloadditions on CdSe QDs. (b) Regioselectivity of intermolecular [2 + 2] cycloaddition on CdSe QDs.
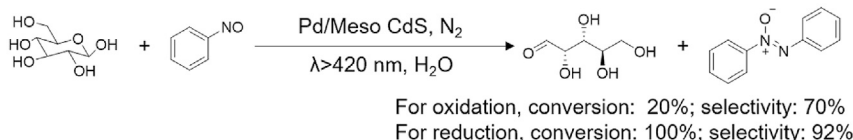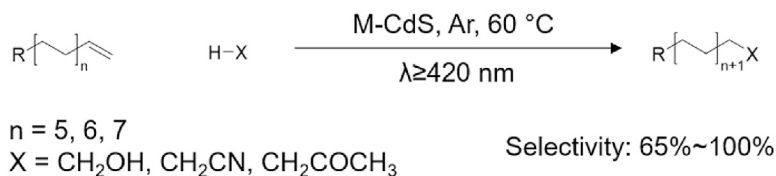

Scheme 34.

Scheme 35.

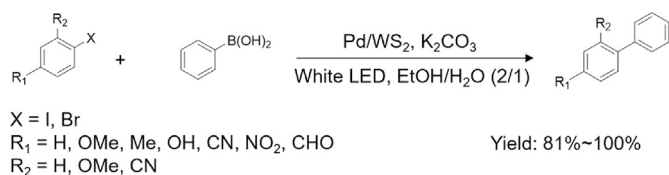abstraction by the superoxide radical (·OOH) led to the final aldehyde product.

Although the above photocatalytic system exhibited good performance for selective benzyl alcohol oxidation, the reaction was conducted under a harsh condition, including high temperature (100 °C) and elevated pressure (8 bar O_2). It is more desirable to carry out this reaction under milder conditions. It has been proved
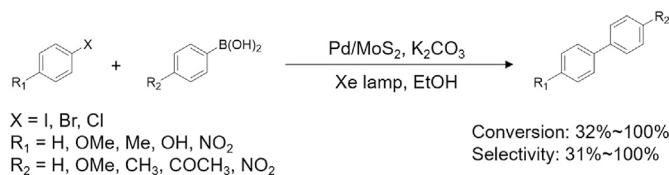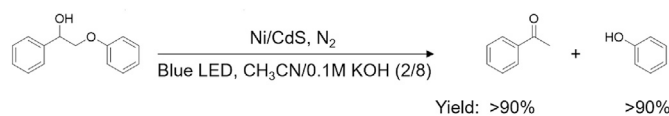

Scheme 36.

Scheme 37.

$$n = 5, 6, 7$$
$$X = CH_2OH, CH_2CN, CH_2COCH_3$$

Selectivity: 65%~100%

X = I, Br
R_1 = H, OMe, Me, OH, CN, NO₂, CHO
R_2 = H, OMe, CN

Yield: 81%~100%

Scheme 38.

Scheme 40.

X = I, Br, Cl
R_1 = H, OMe, Me, OH, NO₂
R_2 = H, OMe, CH₃, COCH₃, NO₂

Conversion: 32%~100%
Selectivity: 31%~100%

Scheme 39.

that doping of metals or non-metal elements is an effective strategy in enhancing the photocatalytic performance of g-C₃N₄ under mild reaction conditions, such as room temperature, atmospheric pressure, and aqueous media (Schemes 42–45) [63].

As aforementioned, oxidation upgrading of biomass-derived alcohols plays a vital role in the development of sustainable

Fig. 16. (a) Reaction path and (b) proposed mechanism of photocatalytic cleavage of a lignin model compound on CdS QDs.

organic synthesis. HMF is a representative biomass-derived platform molecule which can be upgraded into a variety of valuable feedstocks. Photocatalytic oxidation of HMF to DFF is a promising approach alternative to conventional thermal conversions. Several related works have been published on photocatalytic HMF oxidation utilizing carbon nitride as the photocatalyst (Schemes 46–48) [64]. Unfortunately, the obtained DFF yield was mediocre (<40%).

In the photocatalytic oxidation of alcohols to ketones and aldehydes, O₂ often acts as an electron scavenger and H₂O₂ is generated during photocatalysis. However, hydroxyl radicals formed from the dissociation of H₂O₂ is highly reactive and it can initiate numerous undesirable reactions, which will lower the reaction selectivity. Therefore, it would be more promising to utilize other electron scavengers which do not generate active radical species. For the first time, Savateev et al. proposed sulfur, instead of O₂, could be used as an electron scavenger for photocatalytic alcohol oxidation with high selectivity [65]. Sulfur can be readily reduced to H₂S in the presence of electrons and protons. Unlike H₂O₂, H₂S as a gas molecule can be easily released from the reaction mixture, therefore, side reactions could be minimized. In addition, H₂S is also a valuable reagent in the production of thiophenol, an important industrial commodity chemical. In Savateev's work, potassium poly(heptazine imide) (K-PHI) was synthesized as the photocatalyst. Under the same reaction condition except sulfur as electron scavenger instead of O₂, the conversion of benzyl alcohol was increased from 29% to 84.4% and the selectivity of benzaldehyde was also enhanced from 70.5% to 99.5% (Fig. 18a). A tentative mechanism was proposed in Fig. 18b. Upon light irradiation, the excited electrons reduced sulfur to a radical anion. Simultaneously, benzyl alcohol was oxidized by excited holes to yield a radical cation. Subsequent hydrogen atom transfer took place between the sulfur radical anion and the benzyl alcohol radical cation. Followed by a proton abstraction, the intermediate benzyl alcohol radical was transformed to benzaldehyde. Moreover, this photocatalytic system was applied in the synthesis of diethyl 2,4,6-trimethylpyridine-3,5-dicarboxylate (a target molecule of Hantzsch ester). A tandem synthesis route was proposed through the generation of 1,4-dihydropyridine as an intermediate (Fig. 18c).

The excellent oxidation power of K-PHI is owing to its highly crystalline structure (Fig. 19a) [66]. K⁺ can act as counter ions for charged nitrogen atoms in K-PHI, resulting in an extremely positive valence band position (+2.6 eV vs. RHE) (Fig. 19b). The Savateev group has employed K-PHI as the photocatalyst and sulfur as the electron acceptor in several organic photocatalytic reactions. For instance, the synthesis of 1,3,4-oxadiazoles, a valuable product for the medicinal chemistry, from *N*-acylhydrazones was achieved with moderate to good yields (Fig. 19c) [67]. In addition, K-PHI is
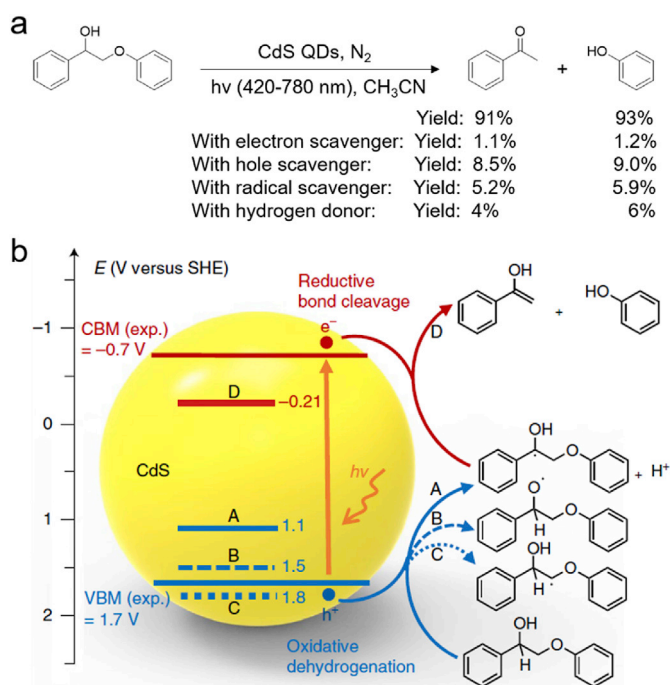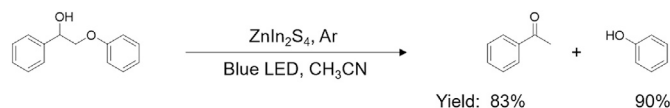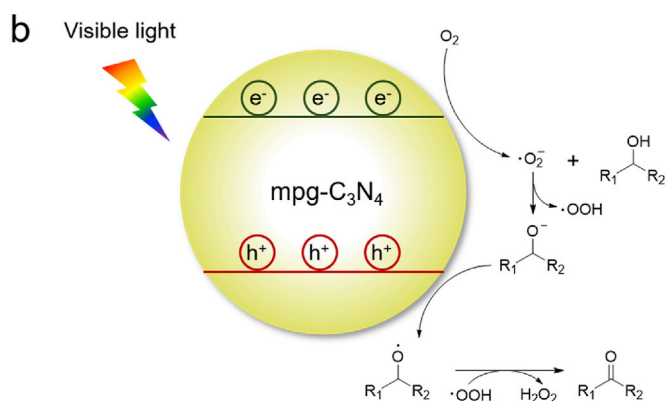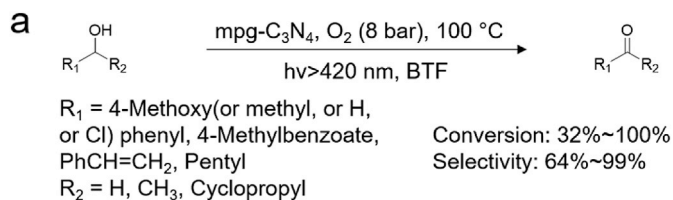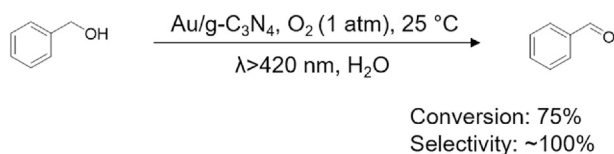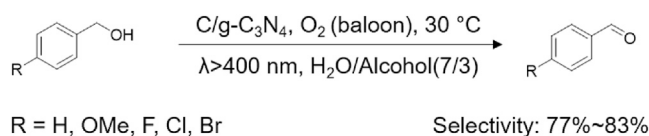
Scheme 41.

Fig. 17. (a) Photocatalytic oxidation of alcohols to their corresponding carbonyls. (b) Proposed mechanism of photocatalytic alcohol oxidation on mpg-C$_3$N$_4$.

able to activate benzylic C—H bonds thanks to its high oxidation power. As an example shown in Scheme 49, sulfur plays two roles, not only acting as an electron scavenger but also being incorporated to the final product dibenzyl disulfides [68]. Another interesting work utilizing the combination of K-PHI and sulfur is the synthesis of thioamide from amine. A series of primary and secondary amines, including substituted benzylamines, heterocyclic, and aliphatic methylamines were successfully converted into thio-amides with excellent yields of 68%−92% (Scheme 50) [69]. A C—N coupling reaction could take place on K-PHI when 2-methylbenzylamine was used as the starting substrate. In this case, only the corresponding coupled imine was isolated as the sole product (Scheme 51).

Besides K-PHI, other carbon nitride-based materials, such as mpg-C$_3$N$_4$ can also oxidize benzylic amines into their correspond-ing imines. Blechert et al. successfully applied mpg-C$_3$N$_4$ as a photocatalyst for the oxidative coupling of benzylic amines [70]. Furthermore, they integrated this oxidative coupling into a one-pot cascade synthesis of industrially important compounds like ben-zoixazoles, benzinidazoles, and benzothiazoles with decent yields (Schemes 52−53). It should be noted relatively high temperature (80 °C and above) was typically required for these reactions. Li et al. proved that carbonyl-modified g-C$_3$N$_4$ (m-O-C$_3$N$_4$) could be an efficient photocatalyst for the oxidative coupling of amines at room temperature with an extremely high yield of ~99% (Scheme 54) [71]. It was rationalized that C=O groups on the photocatalyst surface could bind with in situ formed H$_2$O$_2$, which could accelerate

Scheme 42.

Scheme 43.

Scheme 44.

B/g-C$_3$N$_4$, O$_2$ (1 bar), 60 °C
400 nm LED, BTF

Conversion: ~80%
Selectivity: ~100%
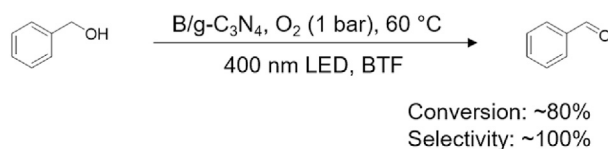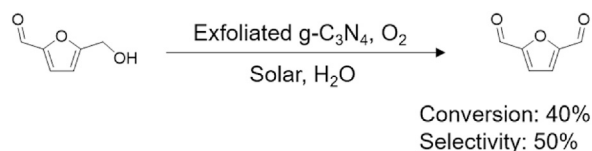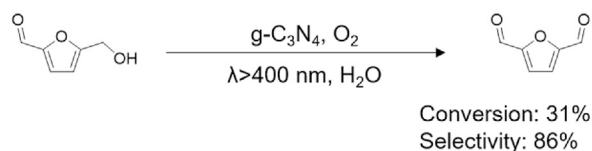
Scheme 45.

Exfoliated g-C$_3$N$_4$, O$_2$
Solar, H$_2$O

Conversion: 40%
Selectivity: 50%

Scheme 46.

g-C$_3$N$_4$, O$_2$
λ>400 nm, H$_2$O

Conversion: 31%
Selectivity: 86%

Scheme 47.

Porous g-C$_3$N$_4$, N$_2$
λ>400 nm, H$_2$O

Yield: 38%
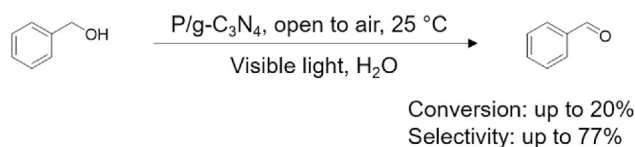
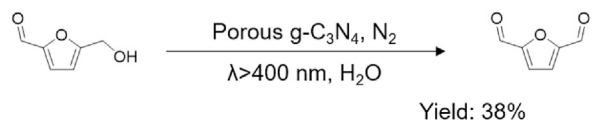**Scheme 48.**

the reaction between H$_2$O$_2$ and amines.

Another promising carbon nitride-based photocatalyst is hexagonal boron carbon nitride (h-BCN), which has been utilized in photocatalytic dehydrogenation reactions [72]. As shown in Scheme 55, an acceptorless dehydrogenation process was realized on h-BCN with H$_2$ as the only byproduct and quinolones could be produced from tetrahydroquinolines. A wide range of substrates with different substituents were successfully converted to the target products with excellent yields, demonstrating the great potential of h-BCN in producing N-containing aromatic compounds under visible light irradiation.

The introduction of K$^+$ can modify the electronic structure of K-PHI and leads to a strong nucleophilicity. Just like K$^+$ in K-PHI, the presence of surface potassium in K-g-C$_3$N$_4$ could also enhance its light-harvesting capability by narrowing the band gap. Therefore, K-g-C$_3$N$_4$ exhibits outstanding performance in visible-light driven oxidative C−C coupling reaction of benzyl alcohol with excellent conversion and selectivity (Scheme 56) [73].

Xie et al. reported that oxidized graphitic carbon nitride (CNO) obtained by incorporating carbonyl groups in carbon nitride could greatly enhance ^{1}O$_2$ generation while suppress the production of other reactive oxygen species [74]. The selective oxidation of sulfide to sulfoxide was chosen as a model reaction (Scheme 57). Compared with pristine g-C$_3$N$_4$, CNO exhibited much higher conversion (99%) and selectivity (~99%). This work not only demonstrated a new excitonic strategy but also provided an efficient

pathway for the design of photocatalyst from the perspective of ^{1}O$_2$ generation. Another photocatalytic oxidation reaction based on g-C$_3$N$_4$ is the direct oxidative esterification of alcohol. For example, Varma et al. prepared a series of g-C$_3$N$_4$ photocatalysts supported with various co-catalysts, including Fe$_3$O$_4$, Pd, Cu, Ag, V$_2$O$_5$, VO, and V(II) [75]. VO/g-C$_3$N$_4$ exhibited the best activity with an ester yield of 98%, much higher than those of the other catalysts. Further, the substrate scope was expanded to include a series of alcohols, including different substituted benzyl alcohols, furfural alcohol and 2-thiophenemethanol, which all showed excellent yields to their corresponding esters (Scheme 58).

4.2. Organic reductive transformations via carbon nitride-based photocatalysts

The aforementioned K-PHI can also drive photocatalytic reductive reactions. Savateev et al. reported the reduction of chalcones using K-PHI as the photocatalyst and triethanolamine (TEOA) as the electron donor [76]. A long-lived radical species of K-PHI was generated, which was beneficial for the generation of chalcones radical through a single-electron reduction process, followed by a reductive cyclodimerization. The regioselectivity was studied by investigating different substituted chalcones. Cyclopentanoles could be produced with 31%−73% isolated yields. In the presence of strong electron-donating groups (e.g., 4-MeOC$_6$H$_4$ or thiophen-2-yl), the major product was dienones. The bulky
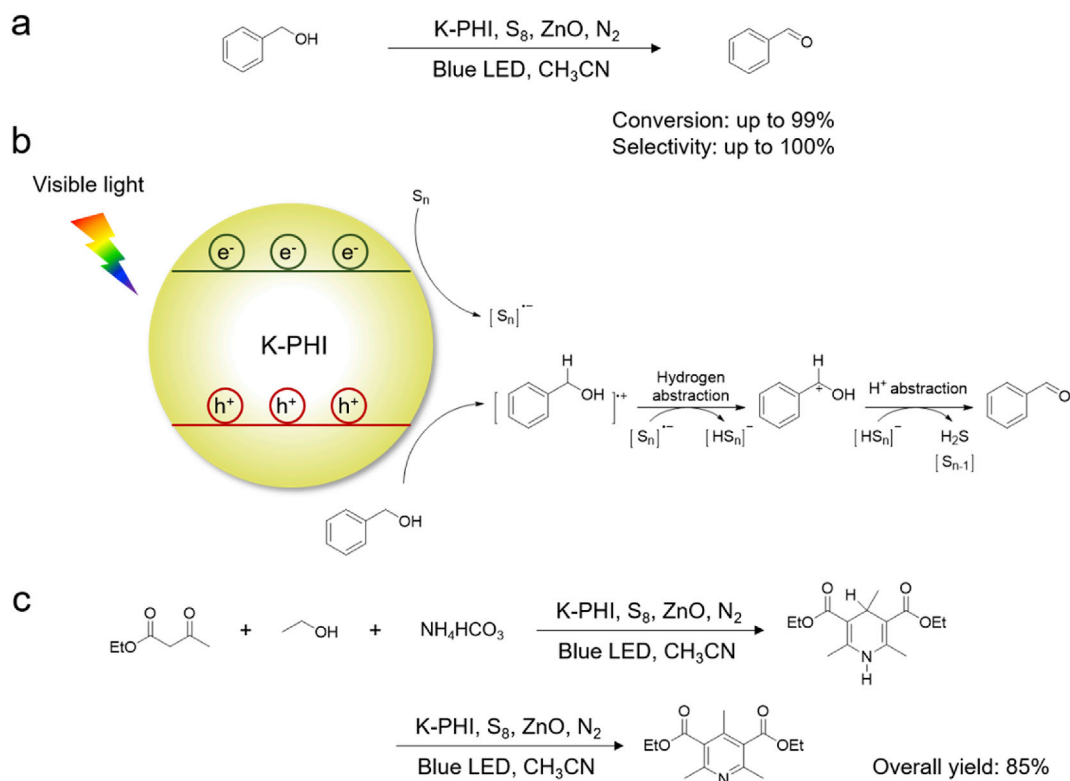
Fig. 18. (a) Photocatalytic oxidation of benzyl alcohol to benzaldehyde on K-PHI with S_8 as an electron scavenger. (b) Proposed mechanism of benzyl alcohol oxidation using K-PHI as photocatalyst and S_8 as electron acceptor. (c) Tandem synthesis of diethyl 2,4,6-trimethylpyridine-3,5-dicarboxylate.
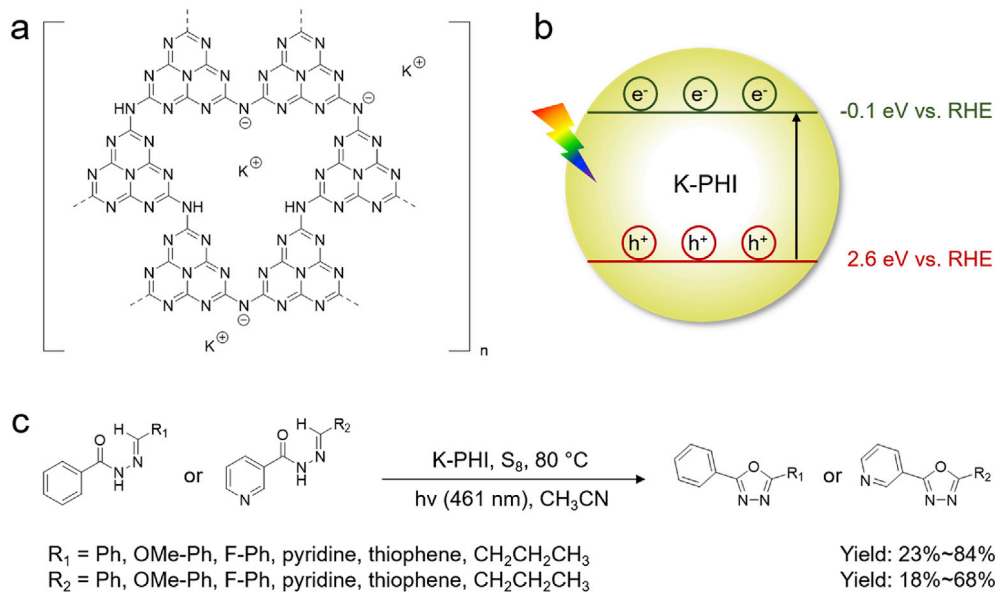
Fig. 19. (a) Molecular structure of K-PHI. (b) Band structure of K-PHI. (c) Photocatalytic oxidation of *N*-acylhydrazones to 1,3,4-oxadiazoles.

pentafluorophenyl substituted chalcone led to the formation of symmetric dimer (yield = 65%) owing to the steric effect (Scheme 59). The same group also reported an unusual photocatalytic addition of dichloromethyl radicals to enones on K-PHI, in which chloroform acted as the source of dichloromethyl radicals [77]. Up to 15 γ,γ-dichloroketones were successfully isolated in moderate to excellent yields (Scheme 60).

Amphiphilic g-C_3N_4 nanosheets decorated with both

R₁ = H, OMe, NHBoc, F, I, CN
R₂ = H, Me

K-PHI, S₈, 50 °C
hv (461 nm), CH₃CN

Yield: 3%~67%

Scheme 49.

R = Ph, Me-Ph, OMe-Ph, NH₂-Ph, pyridine, furan, CH₃CH₂, CH₃CH₂CH₂

K-PHI, S₈, 70 °C
hv (461 nm), dioxane

Yield: 68%~92%

Scheme 50.

K-PHI, S₈, 70 °C
hv (461 nm), dioxane

Isolated product

Scheme 51.

R₁ = H, OMe, Me, Cl, CF₃
R₂ = PhCH₂, Ph, CH₂CH₂, CH(CH₃)₂

mpg-C₃N₄, O₂, 80 °C
λ>420 nm, CH₃CN

Conversion: 46%~99%
Selectivity: 80%~99%

Scheme 52.

R₃ = H, OMe, Me, Cl
X = O, S, NCH₃

mpg-C₃N₄, O₂, 100 °C
λ>420 nm, CH₃CN

Conversion: 70%~99%
Selectivity: 24%~98%

Scheme 53.

m-O-C₃N₄, O₂, RT
hv (420 nm), CH₃CN

Yield: up to 99%

Scheme 54.

hydrophilic and hydrophobic functionalities have been employed in the photocatalytic reduction of nitrobenzene to aniline in a biphasic solution without stirring [78]. As a phase-boundary photocatalyst, the exfoliated g-C₃N₄ nanosheets can be well dispersed at the oil-water biphasic interface. It drives the reduction of nitrobenzene in the oil phase while the produced aniline is more soluble in the aqueous phase, therefore, eliminating the product

R₁ = H, OMe, Me, OH, F, NO₂, COOH
R₂ = H, Me

h-BCN, Ar
Blue LED, H₂O

Yield: 41%~95%

Scheme 55.

Scheme 56.

R_1 = Ph, *p*-Cl (Br, MeO)Ph, *o*-BrPh, CH₃
CH₃CH₂, H, OMe, Me, OH, NH₂, CN
R_2 = Ph, CH₃, CH₃CH₂

CNO: Conversion: 99% Selectivity: 98%~99%
g-C₃N₄: Conversion: 42%~82%;
Selectivity: 10%~55%

Scheme 57.

R_1 = H, OMe, Me, OH, NH₂, CN; X = S, O
Alcohol: CH₃OH, CH₃CH₂OH, (CH₃)₂CHOH

Yield: 76%~99%

Scheme 58.

R = 4-MeOC₆H₄
thiophen-2-yl

R = Ph, 4-MeC₆H₄, 4-FC₆H₄
3-FC₆H₄, 4-CF₃C₆H₄,
3-CF₃C₆H₄, furan-2-yl
3,4-diFC₆H₄

Yield: 42%~53%   Yield: 31%~73%   Yield: 65%
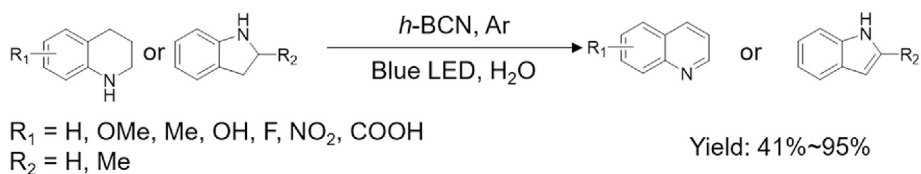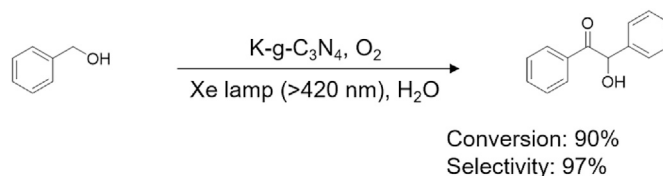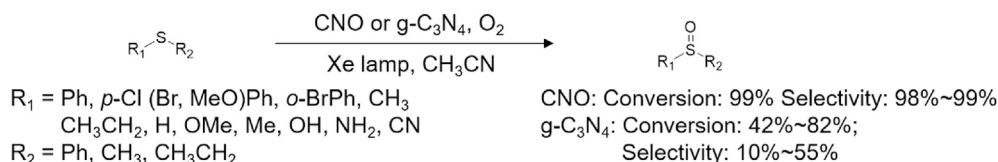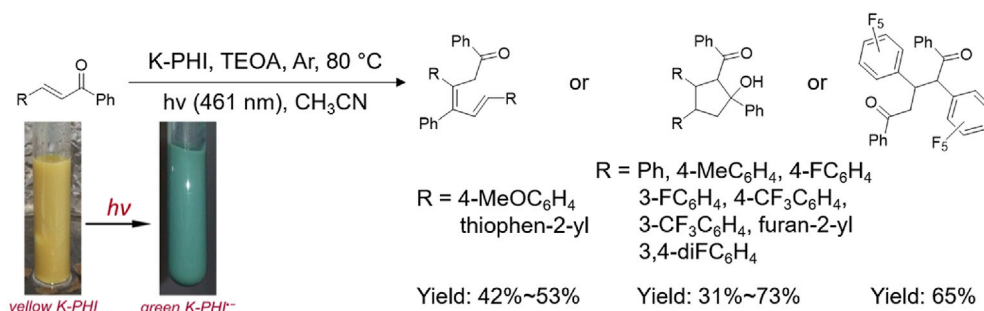
Scheme 59.

separation step and resulting in high yields (>95%) for many substituted nitrobenzene compounds (Scheme 61). Roy et al. compared the physical properties of exfoliated g-C₃N₄ prepared by different methods and found that thermally exfoliated g-C₃N₄ had

much higher surface area and porosity compared to chemically exfoliated g-C₃N₄, leading to a higher rate of nitrobenzene reduction [79]. However, the selectivity of aniline was found to be higher on chemically exfoliated g-C₃N₄, whereas the thermally exfoliated counterpart favored the production of phenyl hydroxyl amine.

A selective photocatalytic approach for the synthesis of industrially important azo- or azoxy-aromatic compound from nitrobenzene was proposed by Su et al. [80]. The selectivity could be readily tuned by simply varying irradiation wavelength when g-C₃N₄ wa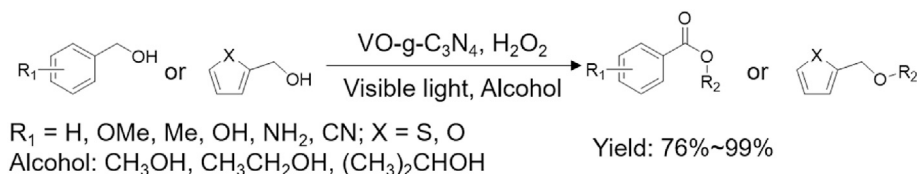s used as the photocatalyst. Upon irradiation at 450 nm, the major product was an azoxy-aromatic compound. In contrast, under the irradiation of 410 nm, an azo-compound was produced as the major product (Scheme 62). More attractively, this photocatalytic system demonstrated a great potential for large scale application. Even up to an 80 L reaction, azoxybenzene could still be formed with high conversion (~60%) and selectivity (~90%) under the irradiation of solar spectrum.

R_1 = Me, C₆H₅, 4-BrC₆H₄
R_2 = H, OMe, Me, F, CF₃, Cl, I, COOMe, CN
X= O, S

Yield: 8%~89%

Scheme 60.

Scheme 61.

R = H, OMe, Me, Cl, CF$_3$

Scheme 62.

For oxidation, conversion: 48%; yield: 45%
For reduction, conversion: 49%; yield: 26%
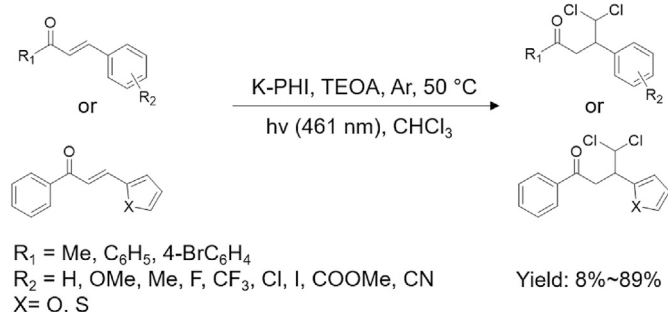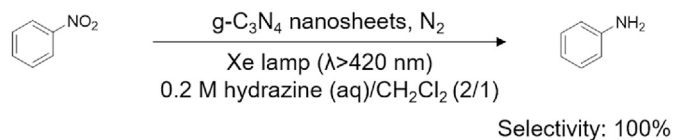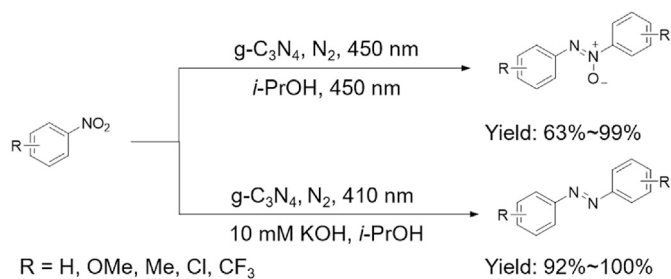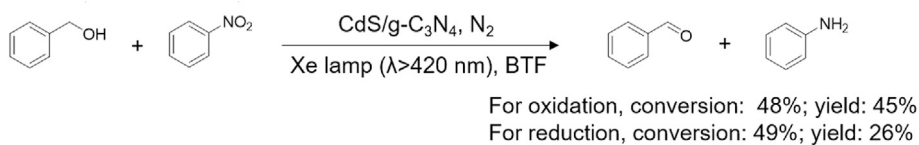
Scheme 63.

Fig. 20. (a) Reaction path of a photocatalytic ketalization reaction catalyzed by g-C$_3$N$_4$. (b) Proposed reaction mechanism of MV^{2+}-mediated photocatalytic ketalization of ketones with methanol.

X = I, Br
R$_1$ = H, OMe, Me, OH, F, I, CF$_3$
R$_2$ = H, OMe, CF$_3$

Yield: 20%~98%
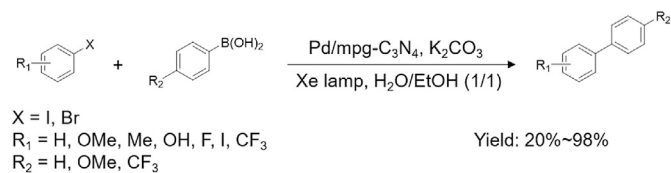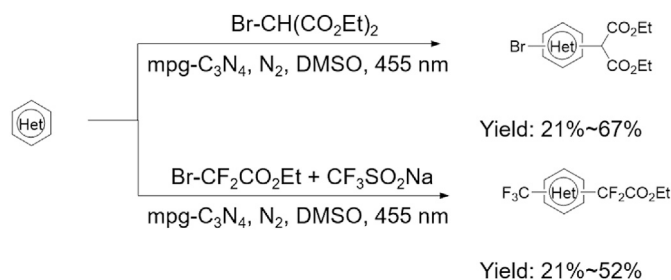
Scheme 64.

Scheme 65.

4.3. Redox-coupled reactions via carbon nitride-based photocatalysts

A coupled system of selective benzyl alcohol oxidation and nitrobenzene reduction was realized by Chen et al. utilizing composite photocatalyst [81]. Compared to pure CdS and g-C_3N_4, the CdS/g-C_3N_4 composite shows great enhancement in photocatalytic property owing to the synergic effect of g-C_3N_4 and CdS, which can facilitate the separation between excited electrons and holes (Scheme 63).

Zhao et al. developed a novel photocatalytic route for ketalization reaction with high reaction rate and selectivity (Fig. 20a) [82]. The high efficiency was owin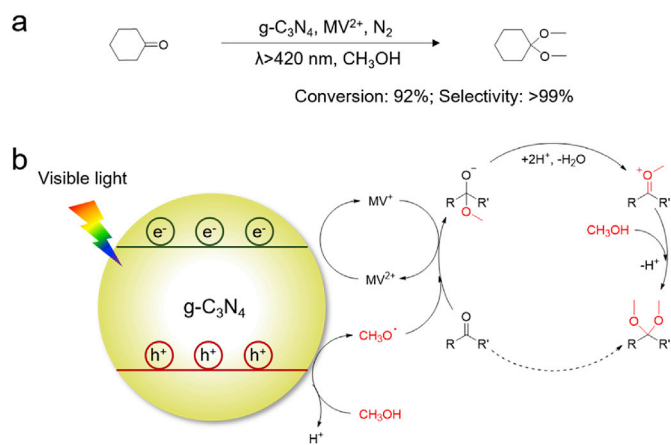g to the fast separation of excited charges facilitated by methylviologen (MV^{2+}) and methanol. In this work, MV^{2+} was an electron mediator and methanol acted as both reactant and hole scavenger. A tentative mechanism was shown in Fig. 20b. Upon the irradiation of visible light, the generated holes oxidized methanol to active methoxy radical, which reacted with the carbonyl group of a ketone to produce a radical adduct. MV^{2+} captured the excited electrons to its low valence state MV^+, which delivered one electron to ketone-methoxy radical adduct to form an anion. Followed by consecutive protonation, water elimination, and the addition of a secondary methoxy radical, the desirable ketal formed as the final product.

Antonietti et al. proposed a Mott-Schottky heterojunction photocatalyst, Pd/g-C_3N_4 for Suzuki C—C coupling [83]. This photocatalyst has high activity and selectivity towards C—C coupling reaction between aryl halides and arylboronic acid with different functional groups (Scheme 64).

Recently, König et al. reported a generalized strategy for bifunctionalization of arenes and heteroarenes utilizing an organic semiconductor photocatalyst, mpg-C_3N_4 [84]. Their mpg-C_3N_4 can facilitate the simultaneous reductive and oxidative electron transfers to two different substrates for direct functionalization of arenes and heteroarenes. In a two-component system, alkyl bromides provided two functional groups, forming C(sp^2)-C(sp^3)/C(sp^2)-Br product by functionalizing at two distinct C—H sites. In a three-component system, two functional groups came from different substrates, generating C(sp^2)-C(sp^3)/C(sp^2)-C(sp^3) as the major product (Scheme 65).

5. Conclusions and outlooks

In this review, we have summarized the development of heterogeneous photocatalysis for a variety of organic transformations. Three classes of well-established semiconductors including metal oxides, metal chalcogenides, and graphitic carbon nitrides are discussed. Although numerous elegant works based on these semiconductors have been reported, there are still several limitations that need improvement. For instance, metal oxides are usually inexpensive and robust, however most of them only absorb in the UV region. In contrast, metal chalcogenides tend to exhibit better visible light absorption, however their long-term stability is a concern. As a metal-free photocatalyst, carbon nitride has attracted increasing attention, while its overall activity is yet to be well documented. Therefore, it is desirable to develop new and competent semiconductors. Firstly, it is desirable to enlarge the scope of useful semiconductors with high activity, stability, and selectivity, especially with non-toxic and inexpensive components. For example, it could be a promising approach to designing composite structures which take advantages of different semiconductors. Secondly, at this moment, the reaction rate and quantum yield are generally low, which are hard to meet the standards of industrial production. In order to improve these two important parameters, it is necessary to design more efficient photocatalysis system, such as the assembly of large-scale device preferably a flow reactor. Thirdly, to fully utilize solar spectrum, new strategies need to be developed to increase the light harvesting ability of photocatalyst to utilize longer wavelengths of light ($\lambda > 500$ nm).

From the aspect of organic reactions, we have presented three reaction types, including oxidation reaction driven by excited holes, reduction reaction driven by excited electrons and redox-coupled reaction utilizing both excited species simultaneously. Several important oxidation reactions driven by excited holes have been well explored, including alcohol oxidation, C—H activation, oxidative C—C coupling, and amine oxidation. Nevertheless, the scope of reduction reactions is still quite limited. Most published reduction works are related to nitrobenzene reduction. However, besides nitrobenzene reduction, there are many other important reduction reactions that await to be explored on semiconductor-based photocatalysts, such as Diels-Alder reaction. In the end, in order to fully utilize the oxidation and reduction power of an irradiated semiconductor simultaneously, it is more appealing to perform redox coupled reactions in one system. This field is still at its infant stage and only a few works have been published. Reported redox coupled reactions are mainly simple transformations like benzyl alcohol oxidation coupled with nitrobenzene reduction and benzyl alcohol hydrogenation coupled with its dehydrogenation. Therefore, it is highly desirable to explore more challenging yet useful organic reactions in a coupled manner. Moreover, one could even envisage a tandem approach both utilizing excited electrons and holes to synthesize more complex molecules with pharmaceutical relevance.

Overall, it remains a long way ahead before heterogeneous photocatalysis can be widely employed in large-scale applications. This calls for the rising interest in photocatalytic organic transformations on semiconductors and more exciting results in this burgeoning field can be certainly expected.

Declaration of competing interest

The authors declare that they have no known competing financial interests or personal relationships that could have appeared to influence the work reported in this article.

References

[1] a) N.S. Lewis, D.G. Nocera, Powering the planet: chemical challenges in solar energy utilization, Proc. Natl. Acad. Sci. U. S. A 103 (2006) 15729–15735;

b) H.B. Gray, Powering the planet with solar fuel, Nat. Chem. 1 (2009) 7;
c) S. Chu, A. Majumdar, Opportunities and challenges for a sustainable energy future, Nature 488 (2012) 294–330;
d) V.S. Thoi, Y. Sun, J.R. Long, C.J. Chang, Complexes of earth-abundant metals for catalytic electrochemical hydrogen generation under aqueous conditions, Chem. Soc. Rev. 42 (2013) 2388–2400.

[2] A. Fujishima, K. Honda, Electrochemical photolysis of water at a semiconductor electrode, Nature 238 (1972) 37–38.

[3] a) C.K. Prier, D.A. Rankic, D.W.C. MacMillan, Visible light photoredox catalysis with transition metal complexes: applications in organic synthesis, Chem. Rev. 113 (2013) 5322–5363;
b) M.H. Shaw, J. Twilton, D.W.C. MacMillan, Photoredox catalysis in organic chemistry, J. Org. Chem. 81 (2016) 6898–6926;
c) J. Twilton, C. Le, P. Zhang, M.H. Shaw, R.W. Evans, D.W.C. MacMillan, The merger of transition metal and photocatalysis, Nat. Rev. Chem. 1 (2017): 0052.

[4] a) J. Kou, C. Lu, J. Wang, Y. Chen, Z. Xu, R.S. Varma, Selectivity enhancement in heterogeneous photocatalytic transformations, Chem. Rev. 117 (2017) 1445–1514;
b) G. Palmisano, V. Augugliaro, M. Pagliaro, L. Palmisano, Photocatalysis: a promising route for 21st century organic chemistry, Chem. Commun. 33 (2007) 3425–3437;
c) X. Lang, X. Chen, J. Zhao, Heterogeneous visible light photocatalysis for selective organic transformations, Chem. Soc. Rev. 43 (2014) 473–486;
d) N. Corrigan, S. Shanmugam, J. Xu, C. Boyer, Photocatalysis in organic and polymer synthesis, Chem. Soc. Rev. 45 (2016) 6165–6212.

[5] X. Lang, J. Zhao, X. Chen, Visible-light-induced photoredox catalysis of dye-sensitized titanium dioxide: selective aerobic oxidation of organic sulfides, Angew. Chem. Int. Ed. 55 (2016) 4697–4700.

[6] Z. Wang, X. Lang, Visible light photocatalysis of dye-sensitized TiO₂: the selective aerobic oxidation of amines to imines, Appl. Catal. B Environ. 224 (2018) 404–409.

[7] X. Li, J.-L. Shi, H. Hao, X. Lang, Visible light-induced selective oxidation of alcohols with air by dye-sensitized TiO₂ photocatalysis, Appl. Catal. B Environ. 232 (2018) 260–267.

[8] A.M. Nauth, E. Schechtel, R. Dören, W. Tremel, T. Opatz, TiO₂ Nanoparticles functionalized with non-innocent ligands allow oxidative photocyanation of amines with visible/near-infrared photons, J. Am. Chem. Soc. 140 (2018) 14169–14177.

[9] L. Ren, M.-M. Yang, C.-H. Tung, L.-Z. Wu, H. Cong, Visible-light photocatalysis employing dye-sensitized semiconductor: selective aerobic oxidation of benzyl ethers, ACS Catal. 7 (2017) 8134–8138.

[10] S. Dana, P. Dey, S.A. Patil, M. Baidya, Enhancing Ru(II)-catalysis with visible-light-mediated dye-sensitized TiO₂ photocatalysis for oxidative C−H olefination of arene carboxylic acids at room temperature, Chem. Asian J. 15 (2020) 564–567.

[11] V. Jeena, R.S. Robinson, Convenient photooxidation of alcohols using dye sensitised zinc oxide in combination with silver nitrate and TEMPO, Chem. Commun. 48 (2012) 299–301.

[12] P. Christopher, H. Xin, S. Linic, Visible-light-enhanced catalytic oxidation reactions on plasmonic silver nanostructures, Nat. Chem. 3 (2011) 467–472.

[13] D. Tsukamoto, Y. Shiraishi, Y. Sugano, S. Ichikawa, S. Tanaka, T. Hirai, Gold nanoparticles located at the interface of anatase/rutile TiO₂ particles as active plasmonic photocatalysts for aerobic oxidation, J. Am. Chem. Soc. 134 (2012) 6309–6315.

[14] A. Tanaka, K. Hashimoto, H. Kominami, Preparation of Au/CeO₂ exhibiting strong surface plasmon resonance effective for selective or chemoselective oxidation of alcohols to aldehydes or ketones in aqueous suspensions under irradiation by green light, J. Am. Chem. Soc. 134 (2012) 14526–14533.

[15] Z. Zheng, B. Huang, X. Qin, X. Zhang, Y. Dai, M.-H. Whangbo, Facile in situ synthesis of visible-light plasmonic photocatalysts M@TiO₂ (M = Au, Pt, Ag) and evaluation of their photocatalytic oxidation of benzene to phenol, J. Mater. Chem. A 21 (2011) 9079–9087.

[16] S.-I. Naya, K. Kimura, H. Tada, One-step selective aerobic oxidation of amines to imines by gold nanoparticle-loaded rutile titanium(IV) oxide plasmon photocatalyst, ACS Catal. 3 (2013) 10–13.

[17] A. Marimuthu, J. Zhang, S. Linic, Tuning selectivity in propylene epoxidation by plasmon mediated photo-switching of Cu oxidation state, Science 339 (2013) 1590–1593.

[18] K. Singha, S.C. Ghosh, A.B. Panda, N-doped yellow TiO₂ hollow sphere-mediated visible-light-driven efficient esterification of alcohol and N-hydroxyimides to active esters, Chem. Asian J. 14 (2019) 3205–3212.

[19] L. Bai, F. Li, Y. Wang, H. Li, X. Jiang, L. Sun, Visible-light-driven selective oxidation of benzyl alcohol and thioanisole by molecular ruthenium catalyst modified hematite, Chem. Commun. 52 (2016) 9711–9714.

[20] C. Zhang, Z. Huang, J. Lu, N. Luo, F. Wang, Generation and confinement of long-lived N-Oxyl radical and its photocatalysis, J. Am. Chem. Soc. 140 (2018) 2032–2035.

[21] R. Yuan, S. Fan, H. Zhou, Z. Ding, S. Lin, Z. Li, Z. Zhang, C. Xu, L. Wu, X. Wang, X. Fu, Chlorine-radical-mediated photocatalytic activation of C-H bonds with visible light, Angew. Chem. Int. Ed. 52 (2013) 1035–1039.

[22] a) C.A. Unsworth, B. Coulson, V. Chechik, R.E. Douthwaite, Aerobic oxidation of benzyl alcohols to benzaldehydes using monoclinic bismuth vanadate nanoparticles under visible light irradiation: photocatalysis selectivity and inhibition, J. Catal. 354 (2017) 152–159;
b) H. Li, F. Qin, Z. Yang, X. Cui, J. Wang, L. Zhang, New reaction pathway

[23] induced by plasmon for selective benzyl alcohol oxidation on BiOCl possessing oxygen vacancies, J. Am. Chem. Soc. 139 (2017) 3513–3521.

[23] Y. Zhang, N. Zhang, Z.-R. Tang, Y.-J. Xu, Identification of Bi₂WO₆ as a highly selective visible-light photocatalyst toward oxidation of glycerol to dihydroxyacetone in water, Chem. Sci. 4 (2013) 1820–1824.

[24] X. Ke, X. Zhang, J. Zhao, S. Sarina, J. Barry, H. Zhu, Selective reductions using visible light photocatalysts of supported gold nanoparticles, Green Chem. 15 (2013) 236–244.

[25] a) H. Zhu, X. Ke, X. Yang, S. Sarina, H. Liu, Reduction of nitroaromatic compounds on supported gold nanoparticles by visible and ultraviolet light, Angew. Chem. Int. Ed. 49 (2010) 9657–9661;
b) S.-C. Li, U. Diebold, Reactivity of TiO₂ rutile and anatase surfaces toward nitroaromatics, J. Am. Chem. Soc. 132 (2010) 64–66.

[26] S. Füldner, R. Mild, H.I. Siegmund, J.A. Schroeder, M. Gruber, B. König, Green-light photocatalytic reduction using dye-sensitized TiO₂ and transition metal nanoparticles, Green Chem. 12 (2010) 400–406.

[27] S. Patai, The Chemistry of the Hydro, Azo and Azoxy, John Wiley & Sons, Ltd, 1997.

[28] Z.-e. Liu, J. Wang, Y. Li, X. Hu, J. Yin, Y. Peng, Z. Li, Y. Li, B. Li, Q. Yuan, Near-infrared light manipulated chemoselective reductions enabled by an unconventional supersandwich nanostructure, ACS Appl. Mater. Interfaces 7 (2015) 19416–19423.

[29] K. Chaiseeda, S. Nishimura, K. Ebitani, Gold nanoparticles supported on alumina as a catalyst for surface plasmon-enhanced selective reductions of nitrobenzene, ACS Omega 2 (2017) 7066–7070.

[30] M. Hosseini-Sarvari, Z. Bazyar, Visible light driven photocatalytic cross-coupling reactions on nano Pd/ZnO at room-temperature, ChemistrySelect 3 (2018) 1898–1907.

[31] Y. Chen, L. Feng, Silver nanoparticles doped TiO₂ catalyzed Suzuki-coupling of bromoaryl with phenylboronic acid under visible light, J. Photochem. Photobiol., B 205 (2020) 111807.

[32] D. Wu, Z. Li, Z. Qi, S. Hu, R. Long, L. Song, Y. Xiong, Boosting photocatalytic activity in cross-coupling reactions by constructing Pd-oxide heterostructure, ChemNanoMat 6 (2020) 920–924.

[33] P. Riente, M.A. Pericàs, Visible light-driven atom transfer radical addition to olefins using Bi₂O₃ as photocatalyst, ChemSusChem 8 (2015) 1841–1844.

[34] L.-M. Zhao, Q.-Y. Meng, X.-B. Fan, C. Ye, X.-B. Li, B. Chen, V. Ramamurthy, C.-H. Tung, L.-Z. Wu, Photocatalysis with quantum dots and visible light: selective and efficient oxidation of alcohols to carbonyl compounds through a radical relay process in water, Angew. Chem. Int. Ed. 56 (2017) 3020–3024.

[35] a) M. Xie, X. Dai, S. Meng, X. Fu, S. Chen, Selective oxidation of aromatic alcohols to corresponding aromatic aldehydes using In₂S₃ microsphere catalyst under visible light irradiation, Chem. Eng. J. 245 (2014) 107–116;
b) S. Meng, X. Ye, X. Ning, M. Xie, X. Fu, S. Chen, Selective oxidation of aromatic alcohols to aromatic aldehydes by BN/metal sulfide with enhanced photocatalytic activity, Appl. Catal. B Environ. 182 (2016) 356–368;
c) X. Ye, Y. Chen, C. Ling, J. Zhang, S. Meng, X. Fu, X. Wang, S. Chen, Chalcogenide photocatalysts for selective oxidation of aromatic alcohols to aldehydes using O₂ and visible light: a case study of CdIn₂S₄, CdS and In₂S₃, Chem. Eng. J. 348 (2018) 966–977;
d) X. Ye, Y. Chen, Y. Wu, X. Zhang, X. Wang, S. Chen, Constructing a system for effective utilization of photogenerated electrons and holes: photocatalytic selective transformation of aromatic alcohols to aromatic aldehydes and hydrogen evolution over Zn₃In₂S₆ photocatalysts, Appl. Catal. B Environ. 242 (2019) 302–311.

[36] X. Sun, X. Luo, X. Zhang, J. Xie, S. Jin, H. Wang, X. Zheng, X. Wu, Y. Xie, Enhanced superoxide generation on defective surfaces for selective photooxidation, J. Am. Chem. Soc. 141 (2019) 3797–3801.

[37] J.L. DiMeglio, A.G. Breuhaus-Alvarez, S. Li, B.M. Bartlett, Nitrate-mediated alcohol oxidation on cadmium sulfide photocatalysts, ACS Catal. 9 (2019) 5732–5741.

[38] G. Han, Y.-H. Jin, R.A. Burgess, N.E. Dickenson, X.-M. Cao, Y. Sun, Visible-light-driven valorization of biomass intermediates integrated with H₂ production catalyzed by ultrathin Ni/CdS nanosheets, J. Am. Chem. Soc. 139 (2017) 15584–15587.

[39] a) A. Lolli, V. Maslova, D. Bonincontro, F. Basile, S. Ortelli, S. Albonetti, Selective oxidation of HMF via catalytic and photocatalytic processes using metal-supported catalysts, Molecules 23 (2018) 2792;
b) H. Zhang, Q. Wu, C. Guo, Y. Wu, T. Wu, Photocatalytic selective oxidation of 5-hydroxymethylfurfural to 2,5-diformylfuran over Nb₂O₅ under visible light, ACS Sustain. Chem. Eng. 5 (2017) 3517–3523;
c) H.-F. Ye, R. Shi, X. Yang, W.-F. Fu, Y. Chen, P-doped Zn_xCd₁₋ₓS solid solutions as photocatalysts for hydrogen evolution from water splitting coupled with photocatalytic oxidation of 5-hydroxymethylfurfural, Appl. Catal. B Environ. 233 (2018) 70–79;
d) B. Ma, Y. Wang, X. Guo, X. Tong, C. Liu, Y. Wang, X. Guo, Photocatalytic synthesis of 2,5-diformylfuran from 5-hydroxymethylfurfural or fructose over bimetallic Au-Ru nanoparticles supported on reduced graphene oxides, Appl. Catal. A-Gen. 552 (2018) 70–76;
e) V.R. Battula, A. Jaryal, K. Kailasam, Visible light-driven simultaneous H₂ production by water splitting coupled with selective oxidation of HMF to DFF catalyzed by porous carbon nitride, J. Mater. Chem. A 7 (2019) 5643–5649;
f) Q. Wu, Y. He, H. Zhang, Z. Feng, Y. Wu, T. Wu, Photocatalytic selective oxidation of biomass-derived 5-hydroxymethylfurfural to 2,5-diformylfuran on metal-free g-C₃N₄ under visible light irradiation, Mol. Catal. 436 (2017)

10−18.

[40] Y. Wang, X. Kong, M. Jiang, F. Zhang, X. Lei, A Z-scheme ZnIn₂S₄/Nb₂O₅ nanocomposite: constructed and used as an efficient bifunctional photocatalyst for H₂ evolution and oxidation of 5-hydroxymethylfurfural, Inorg. Chem. Front. 7 (2020) 437−446.

[41] T. Mitkina, C. Stanglmair, W. Setzer, M. Gruber, H. Kisch, B. König, Visible light mediated homo- and heterocoupling of benzyl alcohols and benzyl amines on polycrystalline cadmium sulfide, Org. Biomol. Chem. 10 (2012) 3556−3561.

[42] K.P. McClelland, E.A. Weiss, Selective photocatalytic oxidation of benzyl alcohol to benzaldehyde or C−C coupled products by visible-light-absorbing quantum dots, ACS Appl. Energy Mater. 2 (2019) 92−96.

[43] N. Luo, T. Hou, S. Liu, B. Zeng, J. Lu, J. Zhang, H. Li, F. Wang, Photocatalytic coproduction of deoxybenzoin and H₂ through tandem redox reactions, ACS Catal. 10 (2020) 762−769.

[44] G. Han, X. Liu, Z. Cao, Y. Sun, Photocatalytic pinacol C-C coupling and jet fuel precursor production on ZnIn₂S₄ nanosheets, ACS Catal. 10 (2020) 9346−9355.

[45] F. Raza, J.H. Park, H.-R. Lee, H.-I. Kim, S.-J. Jeon, J.-H. Kim, Visible-light-driven oxidative coupling reactions of amines by photoactive WS₂ nanosheets, ACS Catal. 6 (2016) 2754−2759.

[46] J.L. DiMeglio, B.M. Bartlett, Interplay of corrosion and photocatalysis during nonaqueous benzylamine oxidation on cadmium sulfide, Chem. Mater. 29 (2017) 7579−7586.

[47] L. Ye, Z. Li, ZnIn₂S₄: a photocatalyst for the selective aerobic oxidation of amines to imines under visible light, ChemCatChem 6 (2014) 2540−2543.

[48] Y.R. Girish, R. Biswas, M. De, Mixed-phase 2D-MoS₂ as an effective photocatalyst for selective aerobic oxidative coupling of amines under visible-light irradiation, Chem. Eur. J. 24 (2018) 13871−13878.

[49] A. Pal, I. Ghosh, S. Sapra, B. König, Quantum dots in visible-light photoredox catalysis: reductive dehalogenations and C−H arylation reactions using aryl bromides, Chem. Mater. 29 (2017) 5225−5231.

[50] J.A. Caputo, L.C. Frenette, N. Zhao, K.L. Sowers, T.D. Krauss, D.J. Weix, General and efficient C−C bond forming photoredox catalysis with semiconductor quantum dots, J. Am. Chem. Soc. 139 (2017) 4250−4253.

[51] Z.-W. Xi, L. Yang, D.-Y. Wang, C.-D. Pu, Y.-M. Shen, C.-D. Wu, X.-G. Peng, Visible-light photocatalytic synthesis of amines from imines via transfer hydrogenation using quantum dots as catalysts, J. Org. Chem. 83 (2018) 11886−11895.

[52] Y. Jiang, C. Wang, C.R. Rogers, M.S. Kodaimati, E.A. Weiss, Regio- and diastereoselective intermolecular [2+2] cycloadditions photocatalysed by quantum dots, Nat. Chem. 11 (2019) 1034−1040.

[53] S. Zhang, W. Huang, X. Fu, X. Zheng, S. Meng, X. Ye, S. Chen, Photocatalytic organic transformations: simultaneous oxidation of aromatic alcohols and reduction of nitroarenes on CdLa₂S₄ in one reaction system, Appl. Catal. B Environ. 233 (2018) 1−10.

[54] S. Meng, X. Ning, S. Chang, X. Fu, X. Ye, S. Chen, Simultaneous dehydrogenation and hydrogenolysis of aromatic alcohols in one reaction system via visible-light-driven heterogeneous photocatalysis, J. Catal. 357 (2018) 247−256.

[55] B. Zhou, J. Song, T. Wu, H. Liu, C. Xie, G. Yang, B. Han, Simultaneous and selective transformation of glucose to arabinose and nitrosobenzene to azoxybenzene driven by visible-light, Green Chem. 18 (2016) 3852−3857.

[56] J. Bao, Y. Fan, S. Zhang, L. Zhong, M. Wu, Y. Sun, Hydrofunctionalization of olefins to higher aliphatic alcohols via visible-light photocatalytic coupling, Catal. Lett. 149 (2019) 1651−1659.

[57] F. Raza, D. Yim, J.H. Park, H.-I. Kim, S.-J. Jeon, J.-H. Kim, Structuring Pd nanoparticles on 2H-WS₂ nanosheets induces excellent photocatalytic activity for cross-coupling reactions under visible light, J. Am. Chem. Soc. 139 (2017) 14767−14774.

[58] H.H. Shin, E. Kang, H. Park, T. Han, C.-H. Lee, D.-K. Lim, Pd-nanodot decorated MoS₂ nanosheets as a highly efficient photocatalyst for the visible-light-induced Suzuki−Miyaura coupling reaction, J. Mater. Chem. A 5 (2017) 24965−24971.

[59] X. Wu, X. Fan, S. Xie, J. Lin, J. Cheng, Q. Zhang, L. Chen, Y. Wang, Solar energy-driven lignin-first approach to full utilization of lignocellulosic biomass under mild conditions, Nat. Catal. 1 (2018) 772−780.

[60] G. Han, T. Yan, W. Zhang, Y.C. Zhang, D.Y. Lee, Z. Cao, Y. Sun, Highly selective photocatalytic valorization of lignin model compounds using ultrathin metal/CdS, ACS Catal. 9 (2019) 11341−11349.

[61] N. Luo, M. Wang, H. Li, J. Zhang, T. Hou, H. Chen, X. Zhang, J. Lu, F. Wang, Visible-light-driven self-hydrogen transfer hydrogenolysis of lignin models and extracts into phenolic products, ACS Catal. 7 (2017) 4571−4580.

[62] F. Su, S.C. Mathew, G. Lipner, X. Fu, M. Antonietti, S. Blechert, X. Wang, mpg-C₃N₄-Catalyzed selective oxidation of alcohols using O₂ and visible light, J. Am. Chem. Soc. 132 (2010) 16299−16301.

[63] a) H. Liang, J. Wang, B. Jin, D. Li, Y. Men, Direct growth of Au nanoparticles on g-C₃N₄ for photocatalytic selective alcohol oxidations, Inorg. Chem. Commun. 109 (2019) 107574;
b) W. Zhang, A. Bariotaki, I. Smonou, F. Hollmann, Visible-light-driven photooxidation of alcohols using surface-doped graphitic carbon nitride, Green Chem. 19 (2017) 2096−2100;
c) M. Bellardita, E.I. García-López, G. Marcì, I. Krivtsov, J.R. García, L. Palmisano,

Selective photocatalytic oxidation of aromatic alcohols in water by using P-doped g-C₃N₄, Appl. Catal. B Environ. 220 (2018) 222−233;
d) M. Zhou, P. Yang, S. Wang, Z. Luo, C. Huang, X. Wang, Structure-mediated charge separation in boron carbon nitride for enhanced photocatalytic oxidation of alcohol, ChemSusChem 11 (2018) 3949−3955.

[64] a) I. Krivtsov, E.I. García-López, G. Marcì, L. Palmisano, Z. Amghouz, J.R. García, S. Ordóñez, E. Díaz, Selective photocatalytic oxidation of 5-hydroxymethyl-2-furfural to 2,5-furandicarboxyaldehyde in aqueous suspension of g-C₃N₄, Appl. Catal. B Environ. 204 (2017) 430−439;
b) Q. Wu, Y. He, H. Zhang, Z. Feng, Y. Wu, T. Wu, Photocatalytic selective oxidation of biomass-derived 5-hydroxymethylfurfural to 2,5-diformylfuran on metal-free g-C₃N₄ under visible light irradiation, Mol. Catal. 436 (2017) 10−18;
c) V.R. Battula, A. Jaryal, K. Kailasam, Visible-light-driven simultaneous H₂ production by water splitting coupled with selective oxidation of HMF to DFF catalyzed by porous carbon nitride, J. Mater. Chem. A 7 (2019) 5643−5649.

[65] A. Savateev, D. Dontsova, B. Kurpil, M. Antonietti, Highly crystalline poly(-heptazine imides) by mechanochemical synthesis for photooxidation of various organic substrates using an intriguing electron acceptor-elemental sulfur, J. Catal. 350 (2017) 203−211.

[66] D. Dontsova, S. Pronkin, M. Wehle, Z. Chen, C. Fettkenhauer, G. Clavel, M. Antonietti, Triazoles: a new class of precursors for the synthesis of negatively charged carbon nitride derivatives, Chem. Mater. 27 (2015) 5170−5179.

[67] B. Kurpil, K. Otte, M. Antonietti, A. Savateev, Photooxidation of N-acylhydrazones to 1,3,4-oxadiazoles catalyzed by heterogeneous visible-light-active carbon nitride semiconductor, Appl. Catal. B Environ. 228 (2018) 97−102.

[68] A. Savateev, B. Kurpil, A. Mishchenko, G. Zhang, M. Antonietti, A "waiting" carbon nitride radical anion: a charge storage material and key intermediate in direct C−H thiolation of methylarenes using elemental sulfur as the "S"-source, Chem. Sci. 9 (2018) 3584−3591.

[69] B. Kurpil, B. Kumru, T. Heil, M. Antonietti, A. Savateev, Carbon nitride creates thioamides in high yields by the photocatalytic Kindler reaction, Green Chem. 20 (2018) 838−842.

[70] F. Su, S.C. Mathew, L. Möhlmann, M. Antonietti, X. Wang, S. Blechert, Aerobic oxidative coupling of amines by carbon nitride photocatalysis with visible light, Angew. Chem. Int. Ed. 50 (2011) 657−660.

[71] J.-J. Zhang, J.-M. Ge, H.-H. Wang, X. Wei, X.-H. Li, J.-S. Chen, Activating oxygen molecules over carbonyl-modified graphitic carbon nitride: merging supramolecular oxidation with photocatalysis in a metal-free catalyst for oxidative coupling of amines into imines, ChemCatChem 8 (2016) 3441−3445.

[72] M. Zheng, J. Shi, T. Yuan, X. Wang, Metal-free dehydrogenation of N-heterocycles by ternary h-BCN nanosheets with visible light, Angew. Chem. Int. Ed. 57 (2018) 5487−5491.

[73] X. Sun, D. Jiang, L. Zhang, W. Wang, Alkaline modified g-C₃N₄ photocatalyst for high selective oxide coupling of benzyl alcohol to benzoin, Appl. Catal. B Environ. 220 (2018) 553−560.

[74] H. Wang, S. Jiang, S. Chen, D. Li, X. Zhang, W. Shao, X. Sun, J. Xie, Z. Zhao, Q. Zhang, Y. Tian, Y. Xie, Enhanced singlet oxygen generation in oxidized graphitic carbon nitride for organic synthesis, Adv. Mater. 28 (2016) 6940−6945.

[75] S. Verma, R.B.N. Baig, C. Han, M.N. Nadagouda, R.S. Varma, Oxidative esterification via photocatalytic C−H activation, Green Chem. 18 (2016) 251−254.

[76] B. Kurpil, Y. Markushyna, A. Savateev, Visible-light-driven reductive (cyclo)dimerization of chalcones over heterogeneous carbon nitride photocatalyst, ACS Catal. 9 (2019) 1531−1538.

[77] S. Mazzanti, B. Kurpil, B. Pieber, M. Antonietti, A. Savateev, Dichloromethylation of enones by carbon nitride photocatalysis, Nat. Commun. 11 (2020) 1387.

[78] C. Yao, A. Yuan, Z. Wang, H. Lei, L. Zhang, L. Guo, X. Dong, Amphiphilic two-dimensional graphitic carbon nitride nanosheets for visible-light-driven phase-boundary photocatalysis, J. Mater. Chem. A 7 (2019) 13071−13079.

[79] S. Challagulla, S. Payra, C. Chakraborty, S. Roy, Determination of band edges and their influences on photocatalytic reduction of nitrobenzene by bulk and exfoliated g-C₃N₄, Phys. Chem. Chem. Phys. 21 (2019) 3174−3183.

[80] Y. Dai, C. Li, Y. Shen, T. Lim, J. Xu, Y. Li, H. Niemantsverdriet, F. Besenbacher, N. Lock, R. Su, Light-tuned selective photosynthesis of azo- and azoxy-aromatics using graphitic C₃N₄, Nat. Commun. 9 (2018) 60.

[81] X. Dai, X. Xie, S. Meng, X. Fu, S. Chen, Coupled systems for selective oxidation of aromatic alcohols to aldehydes and reduction of nitrobenzene into aniline using CdS/g-C₃N₄ photocatalyst under visible light irradiation, Appl. Catal. B Environ. 158-159 (2014) 382−390.

[82] Y. Zhao, M. Shalom, M. Antonietti, Visible light-driven graphitic carbon nitride (g-C₃N₄) photocatalyzed ketalization reaction in methanol with methylviologen as efficient electron mediator, Appl. Catal. B Environ. 207 (2017) 311−315.

[83] X.-H. Li, M. Baar, S. Blechert, M. Antonietti, Facilitating room-temperature Suzuki coupling reaction with light: Mott-Schottky photocatalyst for C-C-coupling, Sci. Rep. 3 (2013) 1743.

[84] I. Ghosh, J. Khamrai, A. Savateev, N. Shlapakov, M. Antonietti, B. König, Organic semiconductor photocatalyst can bifunctionalize arenes and heteroarenes, Science 365 (2019) 360−366.